

Sr–Nd Isotopic Evidence of a Heterogeneous Magmatic Source of Alkaline–Carbonatite Rocks of the Odikhincha Alkaline–Carbonatite Massif (Maimecha-Kotui Province, Siberia)

Y. A. Kostitsyn^a, *, A. R. Tskhovrebova^a, I. T. Rass^b, and M. O. Anosova^a

^a *Vernadsky Institute of Geochemistry and Analytical Chemistry, Russian Academy of Sciences, Moscow, 119991 Russia*

^b *Institute of Geology of Ore Deposits, Petrography, Geochemistry and Mineralogy, Russian Academy of Sciences, Moscow, 119017 Russia*

*e-mail: kostitsyn@geokhi.ru

Received June 10, 2023; revised July 17, 2023; accepted August 2, 2023

Abstract—This study focuses on the igneous rocks composing the Odikhincha massif. The massif is typical ring alkaline–ultrabasic massif with carbonatites, second largest in the Maimecha-Kotui province. The Sr–Nd isotopic values of the traps of the Arydzhang Formation and the host dolomites were also determined for comparison. The Rb–Sr isotope system of phlogopite and calcite from the Od-16-19 carbonatite of the Odikhincha massif is disturbed; the obtained age on the mineral isochrone (245 ± 3 Ma) is close to the time of formation of the Siberian traps and rocks of the ultrabasic–alkaline Maimecha-Kotui complex, but the large scatter of analytical points (MSWD = 22) does not allow this date to be considered as reliable. The disturbance of the isotope system is probably related to the fact that the strontium isotope ratio in the fluid was not constant during autometasomatic phlogopitization of carbonatite. The U–Pb isotopic system of titanite and perovskite from the same carbonatite sample Od-16-19 also appeared to be disturbed, since data points formed discordia. The U–Pb age obtained for titanite and perovskite are 244 ± 5 Ma (MSWD = 1.8) and 247 ± 18 Ma (MSWD = 4), respectively. Apparently, the age values provided by the two isotopic systems (245 ± 3 Ma by Rb–Sr and 247 ± 18 and 244 ± 5 Ma by U–Pb) are consistent with each other and reflect the time of metasomatic processes, i.e., phlogopitization and iolitization. Rb–Sr and Sm–Nd isotope data for ultrabasic–alkaline intrusive rocks with carbonatites of the Odikhincha massif and volcanics of the Arydzhang Formation indicate an enriched, relative to the composition of the convecting mantle, isotopically heterogeneous source of their parent melts. This source could be a combination of ultrabasic mantle rocks and rocks of basic composition (basites). The latter played the role of an enriched component. No signs of contamination of the melts with the host sedimentary rocks in situ were found, however, variations of Sr and Nd isotopic ratios in the rocks of the Odikhincha massif may indicate that during the introduction of deep magmas their interaction and substance exchange with the surrounding rocks of the lithosphere continued up to complete solidification of the melts, as indicated by the nature of local isotopic heterogeneity within the Odikhincha intrusion.

Keywords: Maimecha-Kotui Province, carbonatites, ultrabasic alkaline rocks, Rb–Sr, Sm–Nd, U–Pb, Odikhincha, isotopic dating, mantle sources

DOI: 10.1134/S0016702923120030

Many carbonatites are associated in time and space with large igneous provinces (LIPs) (Ernst and Bell, 2010). In particular, the Siberian LIP includes the world's largest Maimecha-Kotui alkaline–ultrabasic–carbonatite province. Carbonatites, like kimberlites, are derivatives of the deepest magmas ascending from the mantle to the upper crustal horizons. Available experimental and geochemical data indicate that near-solidus compositions formed from carbonatized peridotite during partial melting at pressures greater than 3 GPa have carbonatite compositions (Alibert et al., 1983; Dalton and Wood, 1993; Dalton and Presnall, 1998).

The Maimecha-Kotui ultrabasic alkaline province (Fig. 1) includes 35 small intrusive bodies of alkaline

rocks with carbonatites (Egorov, 1969; Kogarko et al., 1995), combined into the Maimecha-Kotui complex and scattered over an area of about 200×300 km on the northern margin of the Siberian Platform, west of the Anabar Antecline, mainly within its western wing.

The timing of magmatism within the Maimecha-Kotui ultramafic alkaline province is of interest from different perspectives. It is important to understand how long (or short) term the process was of formation of dozens of intrusive bodies, which are similar in the set of constituent rocks and scattered over a vast territory in the northeast of the Siberian Platform. It is equally important for understanding the genesis of these rocks whether mainly tholeiitic trap magmatism

was synchronous with the alkaline magmatism. To resolve these issues, it is necessary to carry out the very accurate dating of individual intrusive bodies of the Maimecha-Kotui complex and to establish the time limits of their formation.

One of the major mysteries of these rocks, which is still far from being solved, is what the source of these melts was and what the mechanism was of their simultaneous formation in relatively small portions, while the distances between intrusive bodies were much (orders of magnitude) larger than their sizes.

Magmatism in this province was dated to a narrow time interval of 252–250 Ma ago (Pokrovskiy and Vinogradov, 1991; Kamo et al., 2003; Kogarko and Zartman, 2007).

According to (Egorov, 1991), the Gulinsky Pluton, being the largest massif of the Maimecha-Kotui Province, is a volcanic–plutonic complex; most authors believe that it has the same age as the Maimecha Formation, that crowns the volcanic section of the Maimecha-Kotui Province. The Gulinsky Pluton is located at the boundary between the Siberian Platform and Mesozoic–Cenozoic Khatanga Trough. Determining its age presented some difficulty. The zircon and baddeleyite mineral fractions from carbonatite of Gulinsky Massif yielded discordant U–Pb ages (Kamo et al., 2003) showing, for one thing, signs of partial loss of radiogenic lead. On the other hand, this discordance, could be explained by disequilibrium in the uranium-235 decay series due to a significant initial excess of protactinium-231. The age of carbonatite was therefore calculated only by the $^{206}\text{Pb}/^{238}\text{U}$ ratio and amounted to 250.2 ± 0.3 Ma. The authors of a recent paper (Ivanov et al., 2021) encountered the same difficulty trying to determine the age of the Gulinsky carbonatite using baddeleyite.

The Gulinsky Massif, with an area of about 35×45 km, is apparently also the largest ultramafic–alkaline massif in the world (Kogarko et al., 1995); other intrusive bodies of the province have more modest sizes, from the first hundred meters to the first kilometers. Most of the intrusions have a simple stock-shaped form and more or less identical constituent rocks: earlier phases were represented by hyperbasites,

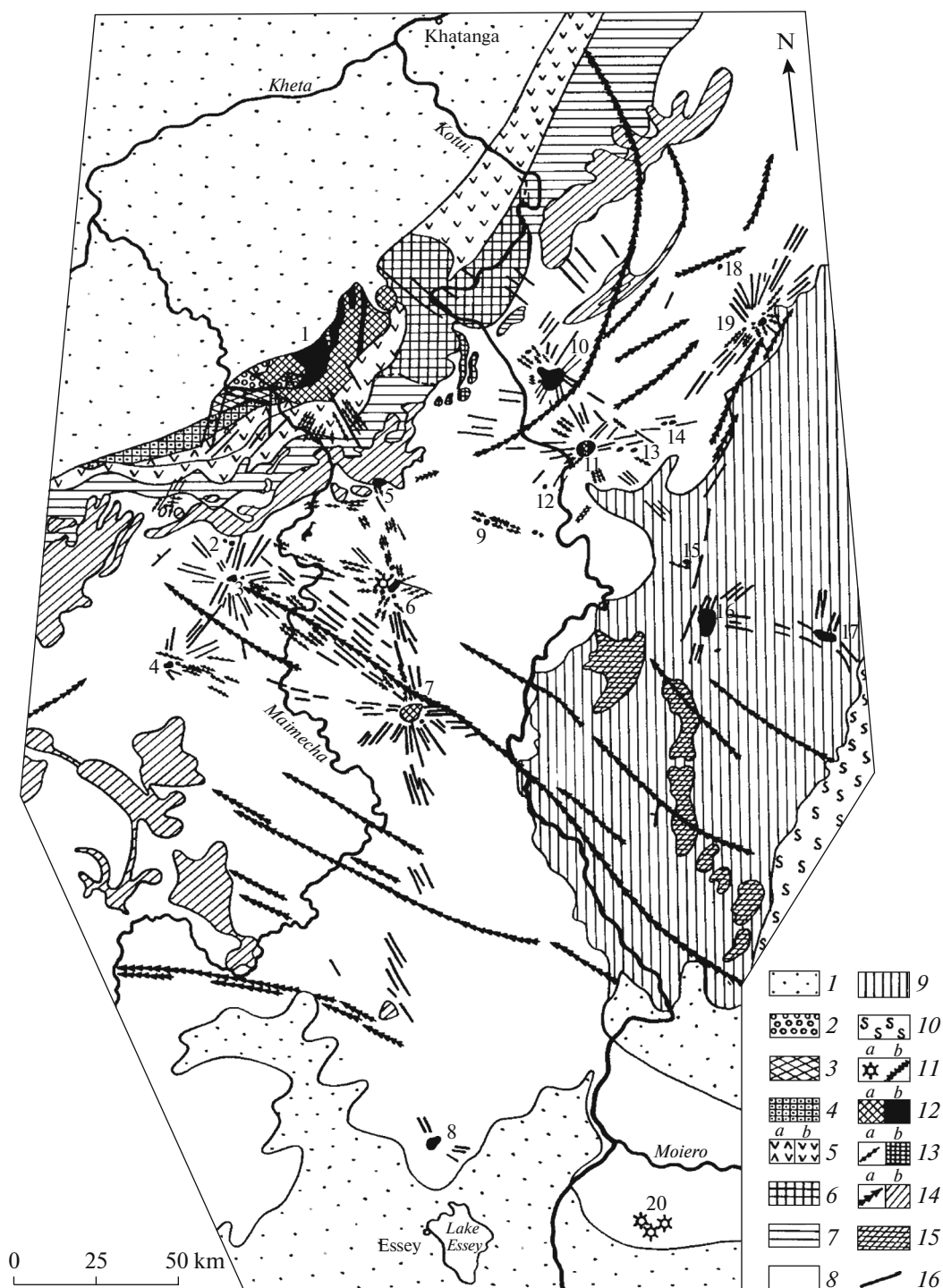
followed by rocks of the melteigite–urtite series and, then, by nepheline and alkaline syenites, phoskorites, and carbonatites (Egorov, 1991).

The age of alkaline basalts of the Arydzhang Formation lying at the base of the volcanic section within the Maimecha-Kotui province, 251.7 ± 0.4 Ma, was determined from the weighted average $^{206}\text{Pb}/^{238}\text{U}$ ratio in 13 perovskite analyses (Kamo et al., 2003).

Isotopic characteristics of meimechites and picrites, apparently the closest in composition to the primary melts of the largest Gulinsky Massif in the Maimecha-Kotui Province (Kogarko et al., 1988), allowed their age to be estimated only in a rather wide time interval of 239 ± 61 Ma and suggested that their source was a result of mixing of depleted mantle and some substrate enriched in lithophile elements. Another hypothesis of their origin suggests a prolonged differentiation of primitive mantle material, including multiple melting, fractionation of solid phases, and distillation of volatile components (Alibert et al., 1983). Subsequent isotopic studies (Kogarko and Zartman, 2007; Kogarko and Zartman, 2011) have determined the age of the Gulin Massif rocks to be 250 ± 9 Ma; combined study of Pb, Sr, and Nd isotopic systems in the Siberian trap rocks and alkaline rocks of the Gulin Massif allowed these authors to actually suggest several components for the source. The first one is a depleted mantle. The second component, representing most of the traps, shows marked chemical and isotopic homogeneity and a similar to chondrite Nd isotopic composition, which made these authors associate it with the lower, primitive mantle. The third and fourth components they term as being contaminated to varying degrees with upper and lower crustal material. Finally, isotopic characteristics of some rocks of the Gulinsky Massif and Siberian plateau basalts with increased SiO_2 content are explained presumably by metasomatic processes (Kogarko and Zartman, 2007).

The published geochronological data obtained by the K–Ar method for the Odikhincha, the second largest massif of the province, are more ambiguous due to a wide range of age values: 225 Ma for phlogopite from olivinite; 245 Ma from pegmatoidal diopside veins and from ijolite–pegmatite (Prokhorova et al,

Fig. 1. Schematic geologic map of the Maimecha-Kotui magmatic province (Egorov, 1991). (1) Mesozoic–Cenozoic sediments; (2–7) volcanic formations of Early Triassic age: (2) meimechites and alkaline metapicrites of the Maimecha Formation, (3) trachybasalts, andesites, and other volcanics of the Verkhnedelkanskaya Subformation, (4) ultramafic phoidites of the Nizhnedelkanskaya Subformation, (5) Kogotok Formation ((a) trachybasalts and trachyandesite–basalts of the Upper Subformation, (b) basalts of the Lower Subformation), (6) ultrabasic phoidites, alkaline picrites, and high-potassium alkaline leucobasalts of the Arydzhang Formation, (7) pyroclastic deposits of the Pravoboyarskaya Formation; (8) essentially carbonate sediments of the Paleozoic; (9) carbonate and terrigenous sediments of the Riphean and Vendian; (10) crystalline rocks of the Archean and Lower Proterozoic; (11–14) intrusive formations of Early Triassic age: (11) kimberlites ((a) diatremes; (b) dikes), (12) rocks of ijolite-carbonatite massifs ((a) ultrabasic; (b) alkaline–ultrabasic and alkaline rocks, foskorites and carbonatites), (13) alkaline–ultrabasic phoidites, alkaline picrites, nephelinites, and phonolites ((a) dikes; (b) sills of alkaline–ultrabasic phoidites), (14) basalts and dolerites ((a) dikes; (b) sills and crosscutting intrusions); (15) dolerites of Riphean age; (16) faults and dikes of presumably alkaline–ultrabasic rocks according to aerial photo interpretation data. Massifs and kimberlite fields (numbers on the map): (1) Gulinsky, (2) Atyrdyak, (3) Romanikha, (4) Changit, (5) Sedete, (6) Dalbykh group of intrusions and kimberlite field, (7) Bor-Uryakh and Kara-Meni, (8) Essey, (9) Krestyakh, (10) Odikhincha, (11) Kugda, (12) Ary-Mas, (13) Sona and Sona-Western, (14) Churbuka, (15) Diogdyoo, (16) Magan, (17) Yraas, (18) Debkoga, (19) Nemakit, (20) Kharamai kimberlite field.



1966); 255 ± 10 and 256 ± 10 Ma for nepheline from urtite and melteigite respectively; and 262 ± 8 and 264 ± 8 Ma for phlogopite from carbonatite and phlogopitized olivinite, respectively (Kononova et al., 1973). Phlogopite from olivinite was dated to 215 Ma, phlogopite from jacupirangite–pegmatite and from ijolite–pegmatite to 233 Ma, and alkaline syenite dyke to 204 Ma (Egorov, 1991). A substantially more accurate

and reliable U–Pb age of 250 ± 1 Ma was obtained from garnet from pegmatoidal rock of the Odikhincha massif by the U–Pb method (Salnikova et al., 2019).

In the present work, we studied the Rb–Sr and Sm–Nd isotope systems of a representative collection of rocks composing the Odikhincha massif, the second largest intrusion of the Maimecha-Kotui Com-

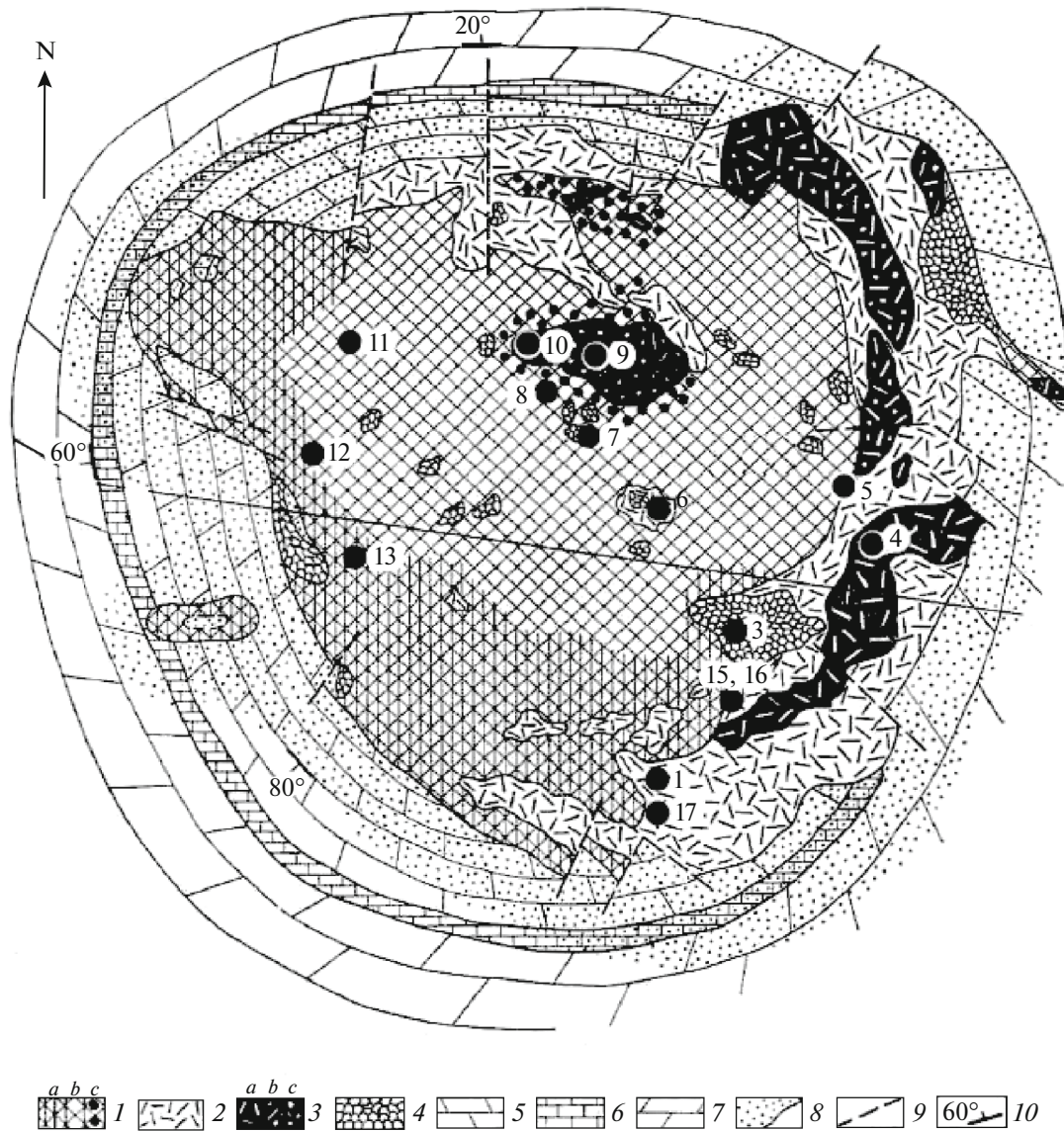


Fig. 2. Schematic geologic map of the Odikhincha intrusion (Egorov, 1969) with rock sampling sites. Sample numbers are given without the Od index (Table 1). Legend: (1) ijolite-melteigites ((a) melteigites, (b) ijolite-urtites, (c) melanitic ijolite), (2) jacupirangite-melteigites, (3) melilitic rocks ((a) uncompahgrites, (b) turjaites, (c) okaites), (4) olivinites, (5) Middle Cambrian dolomites, (6) Lower Cambrian limestones, (7) Upper Cambrian dolomites, (8) halo of contact metamorphism, (9) faults, (10) sedimentary-rock occurrence.

plex, and alkaline basalts of the Arydzhang Formation to evaluate the sources of their parent melts and difference or similarity of the sources of different intrusive rocks of the Maimecha-Kotui Complex.

SAMPLING SCHEME

The Odikhincha massif is a representative typical ring alkaline-ultrabasic carbonatite body within the world's largest Maimecha-Kotui alkaline-ultrabasic province. The massif is located on the watershed of the Kotui River and the Medvezhya River among dolomites of the Mayan Stage of the Middle Cambrian. Its

area is 56 km² (Butakova and Egorov, 1962; Egorov, 1969). The massif was formed in several intrusive phases (Fig. 2). The rocks of the first phase are olivinites and pyroxenites preserved as xenoliths in subsequent differentiates. The second phase is represented by melilite-bearing rocks, uncompahgrites, turjaites, and okaites. They form two large (about 8 km) bodies near the eastern contact—a relatively large (~1 km) body of okaites in the center of the massif and numerous small xenoliths among pyroxene-nepheline rocks of the third phase: jacupirangites, melteigites, ijolite, and ijolite-urtites. All these rocks are intersected by veins of nepheline syenites and carbonatites. All the

above rocks are intensively phlogopitized. Ijolite–melteigites containing numerous xenoliths of olivinites and melilite-bearing rocks are the most widespread in the massif.

We encountered two varieties of carbonatites within the massif: medium-grained calcite carbonatites with phenocrysts of phlogopite and perovskite in the southern part of the massif and pegmatoidal calcite veins with giant, more than 10 cm across, crystals of phlogopite and schorlomite (in the cirque in the central part of the massif). The carbonatite Od-16-19, exposed in a trench in the right side of the Ebe-Yuryakh Creek (Fig. 2), is composed of calcite with small amounts of scattered idiomorphic crystals of phlogopite and rare perovskite. We made an attempt to determine the time of carbonatite crystallization from phlogopite by the Rb–Sr method and from titanite (sphene) and perovskite by the U–Pb method.

We also sampled the other rocks within the massif: phlogopite olivinites, uncomphagrites and melilitolites, melteigites and ijolites, and carbonatites (Table 1). Limburgites and melilitic rocks of the Arydzhang Formation were sampled on the left side of the Kotui River, 3.5 km downstream the mouth of the Medvezhaya River. The coordinates of the sampling sites are given in Table 1. The composition of rocks with respect to petrogenic oxides and trace elements is given in Table 2.

ANALYTICAL PROCEDURE

Isotopic analyses were performed at the Vernadsky Institute of Geochemistry and Analytical Chemistry, Russian Academy of Sciences (GEOKHI RAS), on a Triton TE thermo-ionization mass spectrometer (analysts N.G. Pleshakova and A.R. Tskhovrebova).

Measurement of Nd and Sr isotopic composition with simultaneous determination of Rb, Sr, Sm, and Nd content in rocks and minerals was carried out by isotopic dilution method using mixed tracers $^{85}\text{Rb} + ^{84}\text{Sr}$ and $^{149}\text{Sm} + ^{150}\text{Nd}$. Samples of 20–30 mg and tracers were placed in Teflon containers with 1 mL of a mixture of nitric and hydrofluoric acids in the ratio of 1 : 5, then the containers were placed on a shaker under an infrared lamp for three days. Then, the solutions were evaporated, and 1 mL of strong hydrochloric acid was added and evaporated under an infrared lamp without boiling. This procedure was repeated three times for complete decomposition of fluorides and complete removal of fluorine anion. Then, 1 mL of 2.2 N hydrochloric acid, serving as an eluent for the chromatographic separation of the first-step elements, was added to each sample. The separation of Rb, Sr, and the sum of Sm and Nd with other rare-earth elements was carried out using chromatographic Teflon columns with an inner diameter of 6.2 mm filled with Dowex 50 \times 8 ion-exchange resin up to a height of 90 mm. Elution was performed stepwise: the rubidium

Table 1. Coordinates (WGS84) and nomenclature of the studied rock samples

Sample	N	E	Rock
Dolomites of Mayan Stage (C_{2m})			
Ku-11-14	70.696	103.486	Dolomite
Ku-12-14	70.638	103.369	Marmorized dolomite
Arydzhang Alkaline Basalt			
Ad-1-14	71.182	102.590	Olivine melteigite
Ad-2-14	71.182	102.588	Limburgite
Ad-2a-14	71.183	102.588	Limburgite with calcite geodes
Odikhincha massif			
Od-3-14	70.892	103.145	Biotite olivinite
Od-7-14	70.938	103.122	Pyroxenite
Od-4-14	70.907	103.169	Uncomphagrite
Od-9-14	70.943	103.101	Uncomphagrite
Od-10-14	70.943	103.101	Okaite
Od-6-14	70.936	103.153	Yakupirangite
Od-12-14	70.929	103.037	Ijolite
Od-15-19	70.895	103.137	Ijolite
Od-17-19	70.893	103.095	Ijolite
Od-1-14	70.896	103.105	Ijolite
Od-11-14	70.941	103.053	Urthite
Od-13-14	70.917	103.035	Nepheline syenite
Od-5-14	70.933	103.172	Carbonatit
Od-8-14	70.938	103.111	Pegmatoidal carbonatite
Od-16-19	70.895	103.136	Medium-grained carbonatite

fraction was extracted with 2.2 N HCl, before strontium, then the eluent was changed to 3.9 N hydrochloric acid, to collect strontium and rare-earth elements. Before letting the solution with the sample to the column, it was centrifuged; no precipitate was detected in most cases. The separation of Sm and Nd from the obtained mixture was also carried out by column chromatography with ion-exchange HDEHP (Ln-spec resin) using the columns with an inner diameter of 4 mm and a resin column height of 80 mm. All acids used were prepurified by distillation without boiling. The water was purified by three-stage distillation with boiling.

The Rb–Sr age of carbonatite minerals was determined from individual crystals of calcite and phlogopite (Table 3). Relatively large crystals of mica, more than 30 mg, were split into several pieces with a scalpel and analyzed individually. These analyses are indicated in the table by numbers with decimal points. Phlogopite decomposition was carried out in the same way as the decomposition of whole rocks in general.

Table 2. Content of petrogenic oxides (wt %) and elemental impurities ($\mu\text{g/g}$) in the samples studied

Component	Od-3-14	Od-7-14	Od-4-14	Od-9-14	Od-10-14	Od-6-14	Od-12-14	Od-15-19	Od-17-19	Od-1-14	Od-11-14	Od-13-14
SiO ₂	30.6	42.05	34.91	41.94	39.68	44.63	39.9	42.13	42.24	41.14	39.27	41.91
TiO ₂	1.2	4.55	3.2	0.52	0.69	0.71	1.7	0.97	0.53	1.99	1.15	1.91
Al ₂ O ₃	2.08	5.36	3.82	6.6	17.1	11.98	15.69	15.69	21.07	16.07	18.51	18.82
FeO	15.45	11.21	15.55	7.78	6.20	7.01	11.58	7.79	4.72	10.81	12.13	11.36
MnO	0.361	0.14	0.135	0.092	0.097	0.089	0.144	0.079	0.062	0.128	0.186	0.161
MgO	43.19	11.11	10.06	7.91	5.4	8.92	7.92	7.94	6.21	7.83	5.39	9.28
CaO	0.66	21.94	29.31	29.64	18.52	15.92	11	12.64	10.06	11.7	11.17	10.64
Na ₂ O	0.12	2.76	2.16	3.81	8.84	6.29	8.66	8.09	10.14	8.1	8.98	1.86
K ₂ O	1.72	0.63	0.06	0.15	2.41	1.70	2.86	2.22	3.43	3.01	3.08	4.59
P ₂ O ₅	0.42		0.03	0.00	0.15	0.01	0.05	0.01	0.01	0.02	0.06	0.00
S	0.12					0.14						
LOI	1.92	0.51	0.51	1.25	1.46	1.51	0.51	2.72		0.43		
Sum	97.84	100.26	99.75	99.69	100.55	98.91	100.01	100.28	98.47	100.80	100.36	100.53
XRF:												
V	37.8	40			44	40	69		29	108		
Ni	685	25	41	33.0	24	24	35	41	43.2	22.6	27	59
Co	133	22.0	56	25.5	26	21	28	28	14.2	42.6	21.0	35
Cr	2050			50		27	35	50	29	7.31	50	83
Rb						25	39	34				
Ba	127	104	90	112	148	160	104	152	166	353	200	1100
Sr	24.6	482	2688	2350	3198	372	261	455	348	306	500	494
ICP-MS:												
La	14.2	249	112	145	62	7.3	38	13.6	9.6	37	51	47
Ce	32	539	177	290	113	15.8	80	33	22	69	110	79
Pr	3.5	63	18.1	35	12.6	2.1	8.7	4.3	2.9	7.5	12.7	7.9
Nd	12.1	209	60	116	45	8.5	31	16.7	11.1	27	41	26
Sm	1.27	28	8.8	13.5	6.7	1.61	4.1	2.7	1.68	3.6	4.9	3.6
Eu	0.31	6.5	2.2	3.2	1.88	0.54	1.13	0.76	0.50	1.02	1.26	1.04
Gd	0.79	14.7	5.6	6.4	5.0	1.23	2.6	1.61	1.19	2.5	2.8	2.4
Tb	0.076	1.58	0.56	0.68	0.56	0.140	0.28	0.190	0.130	0.29	0.32	0.29
Dy	0.23	7.7	2.3	2.5	3.1	0.75	1.20	0.82	0.55	1.22	1.64	1.50
Ho	0.038	1.16	0.32	0.34	0.45	0.140	0.200	0.150	0.089	0.23	0.28	0.24
Er	0.110	2.7	0.63	0.68	1.05	0.35	0.50	0.33	0.25	0.46	0.73	0.59
Tm	0.0160	0.29	0.058	0.070	0.100	0.050	0.057	0.050	0.026	0.067	0.100	0.070
Yb	0.094	1.93	0.29	0.26	0.68	0.38	0.37	0.27	0.22	0.42	0.89	0.51
Lu	0.0150	0.25	0.034	0.050	0.080	0.080	0.071	0.060	0.032	0.045	0.170	0.080

Blank cells denote results below the detection limit.

Table 3. Rb–Sr isotope data for individual grains of calcite and phlogopite from Od-16-19 carbonatite

Sample	Rb, ppm	Sr, ppm	$^{87}\text{Rb}/^{86}\text{Sr}$	$^{87}\text{Sr}/^{86}\text{Sr}$	$\pm 2\sigma$
Calcite grains:					
Od-16-19-C1	0.349	9300	0.000108	0.703550	± 14
Od-16-19-C2	0.041	10400	0.000011	0.703583	± 12
Od-16-19-C3	0.035	9660	0.000010	0.703554	± 12
Od-16-19-C4	0.031	9780	0.000009	0.703565	± 12
Od-16-19-C5	0.020	8680	0.000007	0.703569	± 13
Phlogopite grains:					
Od-16-19-F1-1.1	185.8	701	0.766	0.706251	± 13
Od-16-19-F1-1.2 L	202	308	1.892	0.710284	± 13
Od-16-19-F1-1.3	186.1	703	0.766	0.706295	± 12
Od-16-19-F1-2.1	213	548	1.121	0.707484	± 15
Od-16-19-F1-2.2 L	181.4	440	1.193	0.707574	± 13
Od-16-19-F1-2.3	219	583	1.086	0.707371	± 13
Od-16-19-F1-3.1	197.8	250	2.29	0.711367	± 14
Od-16-19-F1-3.2 L	183.3	447	1.187	0.707672	± 15
Od-16-19-F1-5	221	363	1.764	0.709482	± 13
Od-16-19-F1-6	165.0	525	0.715	0.705931	± 13
Od-16-19-F1-7	224	171.6	3.77	0.716616	± 12
Od-16-19-F1-8	178.4	253	2.04	0.710463	± 13
Od-16-19-F1-9	178.4	373	1.382	0.708128	± 14
Od-16-19-F1-10	165.8	367	1.306	0.708072	± 13
Od-16-19-F1-11	153.1	506	0.875	0.706541	± 17
Od-16-19-F1-12	187.1	434	1.247	0.707999	± 15
Od-16-19-F1-13	207	356	1.677	0.709460	± 14

The errors refer to the last digits of the isotopic ratio. L—sample washed in glacial acetic acid. Numbers with a decimal point (e.g., 2.1, 2.2, 2.3) are analyses of different parts of the same phlogopite crystal

Calcite crystals were dissolved in concentrated hydrochloric acid.

Strontium isotopic analysis was carried out in single-filament mode with the addition of a Ta emitter with phosphoric acid; the other elements were analyzed in double-filament mode, using rhenium filament. The measured Nd and Sr isotopic ratios were normalized to $^{148}\text{Nd}/^{144}\text{Nd} = 0.241572$ and $^{86}\text{Sr}/^{88}\text{Sr} = 0.1194$ ratios, respectively. The measured rubidium isotopic ratios were normalized, taking the $^{87}\text{Rb}/^{85}\text{Rb}$ ratio in natural rubidium to be 0.386354 (Villa et al., 2015). The ^{87}Rb decay constant used for calculations was $1.3972 \times 10^{-11} \text{ yr}^{-1}$ (Villa et al., 2015).

The 1% error of the measured Rb/Sr ratio was estimate from simultaneous solution analyses. All errors used in this work have the 95% confidence level. The correctness of the isotopic ratios obtained was controlled by regular analyses of SRM-987 and JNd1 standards (Table 5). The intrinsic convergence in a single experiment in measured isotopic compositions of strontium ($\sim 0.001\%$) and neodymium ($\sim 0.002\%$)

in most cases is markedly less than the reproducibility of strontium and neodymium standards in independent experiments over the entire period of the study ($\sim 0.002\%$ for Sr and $\sim 0.004\%$ for Nd, Table 5). Therefore, the error of each analysis in Tables 3 and 5 is calculated as the root mean square of both errors.

Statistical processing of isochrones was carried out using the York method (York, 1966).

The crystals of perovskite and titanite for U–Pb isotopic study were selected from Od-16-19 carbonatite directly in the field during sampling because their size was the first millimeters. They were embedded in epoxy resin for analysis by LA–ICP–MS. The epoxy mounts with samples were washed in an ultrasonic bath with a working solution (0.5 H HNO₃) to remove surface contamination with common lead. The composition of accessory minerals in the sample was previously studied using a TESCAN MIRA-3 electron microscope at GEOKHI RAS. Isotopic analysis of grains was carried out using the Element XR instrument equipped with an LSX-213 G2+ laser (GEOKHI RAS), the analytical procedure described in detail in (Kostitsyn and

Table 4. LA–ICP–MS U–Pb data for perovskite (*Prv*) and titanite (*Ttn*) from Od-16-19 carbonatite

Sample	Th, ppm	U, ppm	Pb, ppm	Th/U	$^{207}\text{Pb}/^{206}\text{Pb}$	$\pm 1\sigma$	$^{207}\text{Pb}/^{235}\text{U}$	$\pm 1\sigma$	$^{206}\text{Pb}/^{238}\text{U}$	$\pm 1\sigma$	Rho
Od-16-19-Prv-1	3760	622	153	6.04	0.422	0.005	4.74	0.07	0.0814	0.0010	0.69
Od-16-19-Prv-2	1793	646	134	2.77	0.441	0.006	5.15	0.08	0.0845	0.0011	0.69
Od-16-19-Prv-3	1965	679	140	2.89	0.444	0.006	5.12	0.08	0.0837	0.0012	0.69
Od-16-19-Prv-4	1836	435	126	4.22	0.505	0.006	7.12	0.10	0.1022	0.0013	0.70
Od-16-19-Prv-5	2088	468	94	4.46	0.381	0.004	3.95	0.06	0.0751	0.0010	0.70
Od-16-19-Prv-6	1745	594	142	2.94	0.465	0.006	5.80	0.09	0.0903	0.0012	0.68
Od-16-19-Prv-7	1842	421	125	4.37	0.512	0.006	7.26	0.10	0.1029	0.0014	0.71
Od-16-19-Prv-8	900	356	74	2.53	0.444	0.005	5.13	0.07	0.0838	0.0011	0.71
Od-16-19-Prv-9	1721	558	117	3.08	0.424	0.005	4.95	0.07	0.0845	0.0011	0.70
Od-16-19-Prv-10	709	374	71	1.894	0.438	0.005	4.85	0.07	0.0803	0.0011	0.71
Od-16-19-Prv-11	1602	293	65	5.46	0.405	0.005	4.27	0.06	0.0764	0.0010	0.71
Od-16-19-Prv-12	1055	313	83	3.37	0.500	0.006	6.89	0.10	0.1000	0.0014	0.70
Od-16-19-Prv-13	2328	524	131	4.44	0.466	0.005	5.72	0.08	0.0891	0.0012	0.71
Od-16-19-Prv-14	1553	342	67	4.54	0.414	0.005	4.14	0.06	0.0726	0.0010	0.70
Od-16-19-Prv-15	1070	456	83	2.35	0.431	0.005	4.49	0.07	0.0757	0.0010	0.69
Od-16-19-Prv-16	874	455	80	1.920	0.432	0.005	4.50	0.07	0.0755	0.0010	0.69
Od-16-19-Prv-17	748	432	75	1.733	0.429	0.006	4.38	0.07	0.0740	0.0010	0.69
Od-16-19-Prv-18	1971	346	71	5.70	0.381	0.005	3.64	0.06	0.0693	0.0009	0.69
Od-16-19-Prv-19	1671	282	75	5.93	0.468	0.006	5.76	0.09	0.0894	0.0012	0.69
Od-16-19-Prv-20	1134	478	73	2.37	0.365	0.005	3.40	0.05	0.0676	0.0009	0.69
Od-16-19-Prv-21	809	305	57	2.65	0.420	0.005	4.37	0.06	0.0754	0.0010	0.70
Od-16-19-Prv-22	1860	403	80	4.61	0.374	0.005	3.77	0.05	0.0731	0.0010	0.69
Od-16-19-Prv-23	742	359	69	2.07	0.444	0.005	4.88	0.07	0.0797	0.0011	0.70
Od-16-19-Prv-24	617	375	64	1.644	0.414	0.005	4.28	0.06	0.0751	0.0010	0.69
Od-16-19-Prv-25	1197	395	65	3.03	0.366	0.004	3.47	0.05	0.0688	0.0009	0.69
Od-16-19-Prv-26	2076	307	68	6.77	0.384	0.005	3.83	0.06	0.0725	0.0010	0.69
Od-16-19-Prv-27	1402	387	68	3.62	0.369	0.005	3.55	0.05	0.0697	0.0009	0.69
Od-16-19-Ttn-1	12.1	32	1.54	0.380	0.110	0.005	0.61	0.03	0.0400	0.0008	0.59
Od-16-19-Ttn-2	5.3	5.0	0.26	1.069	0.080	0.011	0.44	0.06	0.0399	0.0015	0.56
Od-16-19-Ttn-3	48	11.2	1.91	4.30	0.379	0.015	3.43	0.13	0.0657	0.0016	0.61
Od-16-19-Ttn-4	1.10	1.85	0.37	0.594	0.51	0.04	6.03	0.40	0.086	0.004	0.60
Od-16-19-Ttn-5	56	62	3.7	0.913	0.133	0.003	0.782	0.021	0.0426	0.0007	0.63
Od-16-19-Ttn-6	63	50	2.7	1.259	0.088	0.003	0.477	0.017	0.0391	0.0007	0.60
Od-16-19-Ttn-7	55	88	4.0	0.626	0.082	0.003	0.447	0.014	0.0394	0.0007	0.61
Od-16-19-Ttn-8	77	62	3.2	1.239	0.077	0.003	0.408	0.014	0.0385	0.0007	0.60
Od-16-19-Ttn-9	5.8	5.5	0.26	1.046	0.073	0.009	0.39	0.05	0.0389	0.0013	0.55
Od-16-19-Ttn-10	27	21	1.19	1.327	0.100	0.006	0.59	0.04	0.0425	0.0011	0.58
Od-16-19-Ttn-11	54	51	3.4	1.071	0.148	0.004	0.937	0.025	0.0460	0.0008	0.63
Od-16-19-Ttn-12	50	52	3.2	0.966	0.134	0.004	0.814	0.024	0.0442	0.0008	0.61
Od-16-19-Ttn-13	76	66	3.5	1.159	0.083	0.003	0.462	0.016	0.0406	0.0007	0.60
Od-16-19-Ttn-14	46	39	2.00	1.168	0.082	0.003	0.446	0.017	0.0396	0.0007	0.59
Od-16-19-Ttn-15	3.5	2.6	0.157	1.354	0.093	0.016	0.56	0.09	0.0434	0.0019	0.55
Od-16-19-Ttn-16	5.2	4.6	0.22	1.127	0.062	0.010	0.34	0.05	0.0395	0.0013	0.54

Rho—correlation coefficient for errors of $^{207}\text{Pb}/^{235}\text{U}$ and $^{206}\text{Pb}/^{238}\text{U}$ ratios.

Table 5. Rb–Sr and Sm–Nd isotope data for rock samples and isotope standards

Sample	Rb, ppm	Sr, ppm	$^{87}\text{Rb}/^{86}\text{Sr}$	$^{87}\text{Sr}/^{86}\text{Sr}^{\text{I}}$	$\pm 2\sigma$	$^{87}\text{Sr}/^{86}\text{Sr}(\text{T})$	Sm, ppm	Nd, ppm	$^{147}\text{Sm}/^{144}\text{Nd}$	$^{143}\text{Nd}/^{144}\text{Nd}^{\text{I}}$	$\pm 2\sigma$	$\epsilon_{\text{Nd}}(\text{T})$	T_{Nd2}
Ku-11-14	0.981	38.8	0.0732	0.709026	± 23	0.70877	0.0459	0.249	0.1112	0.51218	± 91	-6.2	
Ku-12-14	0.462	28.8	0.0464	0.709196	± 13	0.70903	0.238	1.344	0.1072	0.51208	± 5	-8.0	
Ad-1-14	11.3	807	0.0407	0.703616	± 13	0.70347	5.34	39.1	0.0826	0.512665	± 26	4.2	0.66
Ad-2-14	13.3	1838	0.0209	0.703624	± 15	0.70355	13.28	97.2	0.0826	0.512670	± 22	4.3	0.65
Ad-2a-14	13.4	3082	0.01262	0.703580	± 15	0.70354	10.04	74.1	0.0819	0.512647	± 22	3.8	0.69
Od-3-14	90	349	0.747	0.707240	± 15	0.70463	5.34	44.2	0.0730	0.512520	± 21	1.7	0.91
Od-7-14	5.1	37	0.398	0.705085	± 13	0.70369	0.261	2.27	0.0696	0.512571	± 22	2.8	0.80
Od-4-14	1.69	2215	0.00221	0.703896	± 15	0.70389	25.1	238	0.0637	0.512516	± 23	1.9	0.89
Od-9-14	11.2	3619	0.00897	0.703405	± 20	0.70337	4.20	30.9	0.0823	0.512650	± 24	3.9	0.69
Od-9-14*	8.1	4652	0.00505	0.703302	± 13	0.70328	10.46	76.5	0.0826	0.512659	± 24	4.1	
Od-10-14	25	2893	0.0253	0.703430	± 23	0.70334	12.64	93.9	0.0814	0.512681	± 21	4.5	0.63
Od-6-14	0.88	7.9	0.322	0.70547	± 15	0.70434	0.469	4.21	0.0673	0.512516	± 22	1.8	0.90
Od-12-14	42	253	0.477	0.705201	± 22	0.70353	1.159	6.56	0.1068	0.512562	± 28	1.4	0.93
Od-15-19	43.0	2228	0.0555	0.704151	± 15	0.70396	60.6	505	0.0726	0.512525	± 24	1.8	0.90
Od-17-19	34.8	999	0.1006	0.704053	± 13	0.70370	12.01	86.5	0.0840	0.512538	± 24	1.6	0.91
Od-1-14	48	438	0.314	0.704862	± 13	0.70376	4.67	34.3	0.0824	0.512536	± 31	1.7	0.91
Od-11-14	66	246	0.777	0.706729	± 14	0.70401	1.081	8.24	0.0793	0.512504	± 23	1.1	0.96
Od-13-14	59	305	0.559	0.706284	± 14	0.70433	2.36	16.55	0.0863	0.512532	± 17	1.5	0.88
Od-5-14	0.47	22408	0.000061	0.704166	± 16	0.70417	0.720	10.9	0.0397	0.512482	± 23	2.0	0.88
Od-8-14	92	163418	0.00162	0.703363	± 15	0.70336	2.05	32.6	0.0380	0.512584	± 26	4.0	0.68
Od-16-19	0.392	9137	0.00012	0.703575	± 14	0.70357	2.34	27.4	0.0517	0.512519	± 22	2.3	0.84
SRM-987 (N = 5)													
JNd1 (N = 5)				0.710235	± 12								

* Retest. The errors refer to the last digits of the isotopic ratio. T_{Nd2} —two-stage Nd model age, Ga.

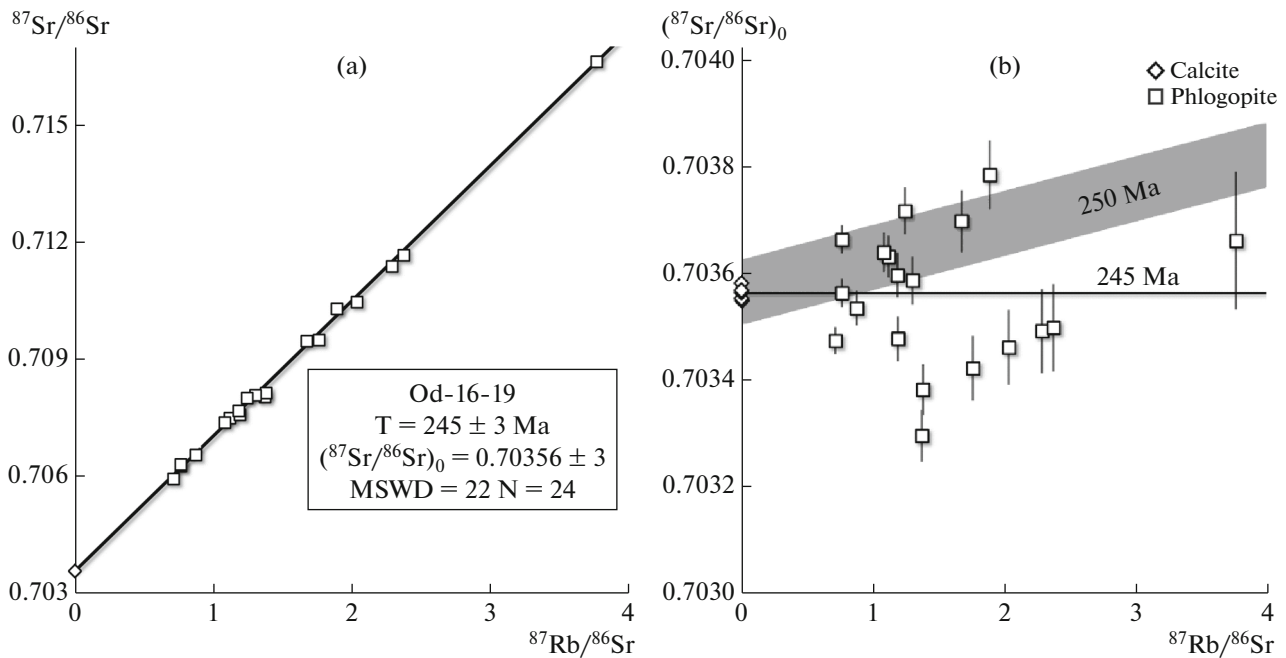


Fig. 3. (a) Isochron for carbonatite Od-16-19; the data points stand for individual grains of calcite and phlogopite. (b) “Residue plot” for the same data. The Rb–Sr mineral system is disturbed and the location of the analytical points does not contradict the fact that the age of the carbonatite is close to 250 Ma.

Anosova, 2013). Apart from the sample, each measurement sequence included GJ and 91500 zircon standards. The measurement parameters were as follows: laser pulse frequency 6 Hz, beam diameter 40 μm , gas flows: Ar (cooling)—16 L/min, Ar (auxiliary)—1.95 L/min, Ar (with sample)—0.975 L/s, He—0.9 L/min. The data obtained were processed using the Glitter software (van Achterbergh et al., 1999).

RESULTS

Rb–Sr Isotope System in Phlogopite and Calcite From Carbonatite Od-16-19

To determine the age of medium-grained carbonatite Od-16-19, collected from a trench in the right bank of the Ebe-Yuryakh River (Fig. 2), we performed Rb–Sr isotopic analyses of carbonatite minerals, five grains of calcite and 12 grains of phlogopite. Three of these grains were split into fragments further analyzed separately (Table 3). The resulting MSWD (Fig. 3) was 22, which definitely indicates that the Rb–Sr isotope system of the minerals was disturbed. At the same time, the dispersion of analytical points relative to the line of best fit is much greater for phlogopite crystals than for calcite crystals, although the observed scatter in strontium isotope ratios of calcite was 6.7 times larger than the error of isotopic analysis.

Figure 3b shows the so-called “residual plot,” the deviation of analytical points from the approximating function, in this case, from the isochrone. The residual plot can be useful for identifying individual anomalously high deviations or for detecting certain patterns

in the scatter of analytical points that may not be visible in the isochron diagram. In this case, however, analytical points are scattered rather chaotically around the line of best fit, which seems to indicate a more or less uniform nature of isotope-system disturbances in all analyzed mineral grains.

U–Pb Isotope System of Perovskite and Titanite From Carbonatite Od-16-19

Concordia diagrams constructed from the U–Pb isotope data obtained for two perovskite crystals and one titanite crystal (Fig. 4) show that the analytical points do not fall on the concordia line, but form discordia. The lower intersections of discordia and concordia probably correspond to the time of the U–Pb system closure. The intersection of discordia with the ordinate axis corresponds to the isotopic ratio $^{207}\text{Pb}/^{206}\text{Pb}$ of common lead these minerals; i.e., discordia in this case represent the lines of mixing of radiogenic and common lead, the latter acting as a contaminant.

The U/Pb ratio in perovskite (Fig. 4a) is generally lower than in titanite (Fig. 4b). The perovskite data points are compactly clustered in the middle part of the plot (Fig. 4a) and are noticeably shifted from the concordia; the age value obtained for this mineral has, therefore, a larger error: 247 ± 18 Ma. The MSWD value is also slightly increased (4.0); i.e., these samples had some analytical “noise” in addition to the analytical error.

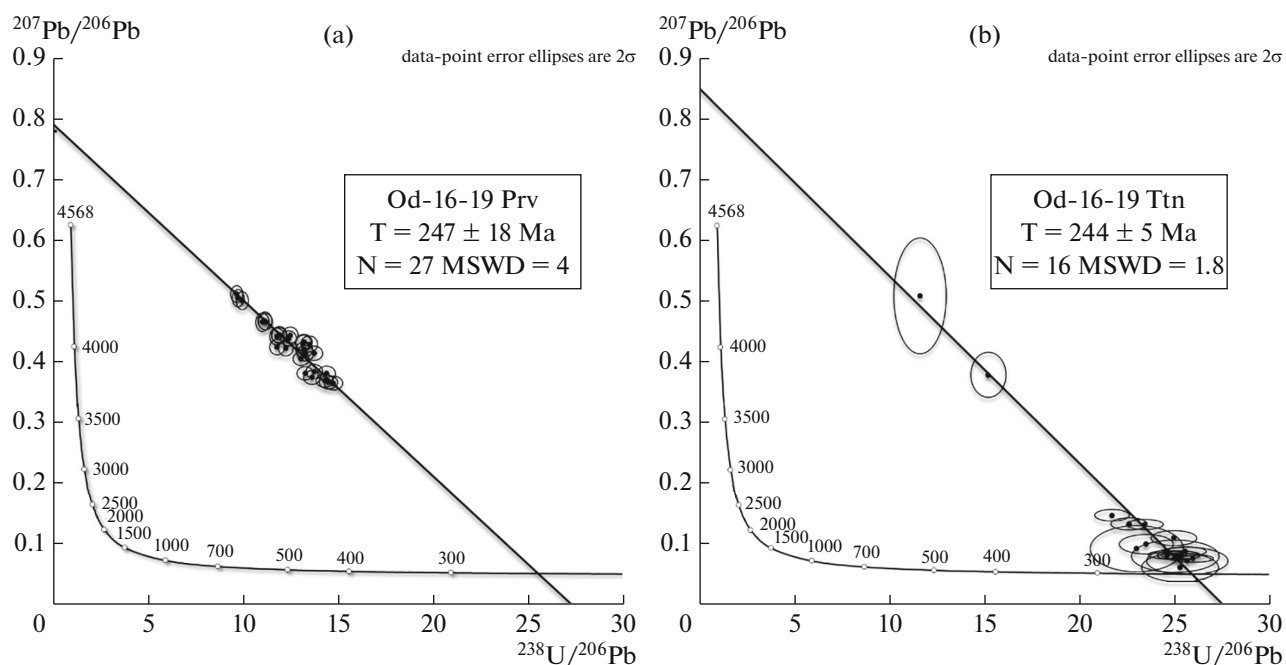


Fig. 4. Tera-Wasserburg diagrams: (a) for perovskite and (b) for titanite crystals from the Od-16-19 carbonatite of the Odikhincha massif.

Since the U–Pb age obtained for titanite was 244 ± 5 Ma with a moderate MSWD of 1.8, it can be assumed that all isotopic data for this mineral are self-consistent.

Geochemistry of Sr and Nd

The Rb–Sr and Sm–Nd isotope data obtained for rocks of the Odikhincha intrusive body, host Upper Cambrian dolomites and basalts of the Arydzhang Formation are presented in Table 5.

The initial (as of 250 Ma ago) isotopic ratios of neodymium and strontium in the igneous rocks of the Odikhincha massif are variable: $\epsilon_{\text{Nd}}(T)$ from +1.1 to +4.5, and $(^{87}\text{Sr}/^{86}\text{Sr})_0$ from 0.7033 to 0.7046. At the same time, no systematic differences in the strontium isotopic composition between the different groups of rocks were revealed (Fig. 5a), whereas a closer look at the neodymium isotopic composition uncovered differences between nepheline-bearing varieties, on the one hand, and other rocks, on the other. Neodymium isotopic ratios in nepheline-bearing rocks (ijolites, jacupirangite, urtite, nepheline syenite) vary within much narrower limits, $\epsilon_{\text{Nd}}(T)$ from +1.1 to +1.8, than in other rock types, including melilite-bearing (uncompahgrites, okaites) and nonmelilite ultrabasites (olivinite and pyroxenite), as well as carbonatites. These samples have significantly wider variations of $\epsilon_{\text{Nd}}(T)$, from +1.7 to +4.5.

The samples of the Arydzhang Formation were rather homogeneous in the Nd and Sr isotopic com-

position: $\epsilon_{\text{Nd}}(T)$ varies from +3.8 to +4.3, and $(^{87}\text{Sr}/^{86}\text{Sr})_0$ varies from 0.70347 to 0.70355. The outcrop they were collected from is located close to section 3 described in (Fedorenko et al., 2000), and our results are in good agreement with the data given in that paper. The samples from the other two sections (sections 1 and 5, in (Fedorenko et al., 2000)) have slightly different isotopic ratios, but, in general, the range of Nd and Sr variations in the Arydzhang Formation volcanics varies within the same limits as in the melilite-bearing rocks of the Odikhincha Formation (Fig. 5a).

In general, the Nd and Sr initial isotopic ratios in the samples of the Arydzhang Formation, Odikhincha massif, and carbonatites of the Gulinsky and Esseï massifs (Morikiyo et al., 2001) reflect a relatively enriched source in comparison with the composition of the convective mantle (Fig. 5b) represented by mid-ocean ridge basalts (MORB). It is not uncommon to associate all neodymium isotopic ratios with values of $\epsilon_{\text{Nd}}(T) > 0$ with geochemically depleted sources, following the model (DePaolo and Wasserburg, 1976), which is of course a misconception. The issue is discussed below.

DISCUSSION

Geochronology

The Rb–Sr System in Carbonatite Minerals

Let us consider the possible causes of the disturbance of the Rb–Sr isotope system of Od-16-19 car-

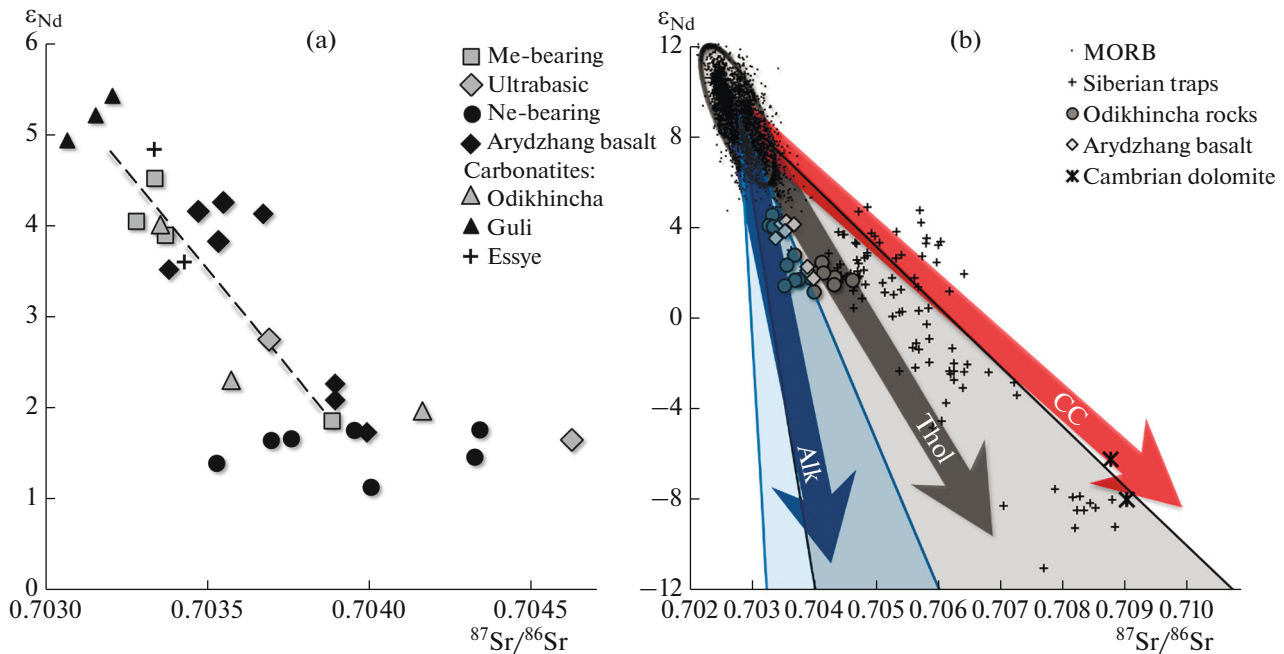


Fig. 5. (a) $\epsilon_{Nd}(T)$ and Sr isotopic ratios in melilite-bearing (Me-bearing), nepheline-bearing (Ne-bearing) ultramafic rocks and carbonatites of the Odikhincha massif, as well as carbonatites of the Essye and Gulinsky massifs (Morikiyo et al., 2001), and alkaline basalts of the Arydzhang Formation, including data from (Fedorenko et al., 2000). The dotted line corresponds to the curves in Fig. 7. (b) The same data compared to the data for the mid-ocean ridge basalts (MORBs, see (Kostitsyn, 2004, 2007)) and Siberian traps (Lightfoot et al., 1993; Wooden et al., 1993; Hawkesworth et al., 1995; Arndt et al., 1998; Krivolutskaya et al., 2012; Kiselev et al., 2014; Reichow et al., 2016); unpublished data of Y.A. Kostitsyn and N.A. Krivolutskaya were also used. There are also compositions of Middle Cambrian dolomites hosting the massif (Table 5). A two-sigma dispersion ellipse is given for MORB. Broad arrows indicate the possible position of ancient enriched sources of initially mantle isotopic composition, but with elemental characteristics (Rb/Sr and Sm/Nd) corresponding to the continental crust (Taylor and McLennan, 1985)—CC (red arrow); median compositions of tholeiitic basalts and gabbro—Thol (gray arrow); and alkaline rocks—Alk (blue arrow); the variation ranges of Rb/Sr and Sm/Nd ratios (Table 5) are shown for the latter two rock types in gray and blue colors, respectively.

bonatite minerals. These could be (a) isotopic heterogeneity in the parent substance (melt/fluid) of the carbonatite minerals and/or (b) long-term mineral crystallization and/or (c) superimposed metamorphic transformations significantly separated in time from the initial formation of the rock.

Microscopic study of minerals gave no signs of secondary alteration of calcite or even phlogopite. In addition, high strontium (8000–10000 ppm) and low rubidium (less than 1 ppm) contents in calcite crystals resulted in extremely low values of Rb/Sr ratio, from 2.4×10^{-6} to 3.8×10^{-5} . Since the addition of radiogenic strontium in calcite over the past ~ 250 Ma would be much smaller than the error of isotope analysis, the Rb–Sr isotopic system of calcite crystals is resistant to superimposed thermal events in the late history of the rock.

At the same time, both phlogopite and calcite crystals contain isotopically heterogeneous strontium: variations in the initial isotopic Sr composition in both groups of minerals several times higher than the analytical error. Apparently, the main reason for the disturbance of the Rb–Sr isotopic system is variable Sr isotopic composition in the parent melt or fluid. Signs of metasomatic alteration (phlogopitization, iolitiza-

tion) of rocks of Odikhincha and other bodies of Mai-mecha-Kotui province are described in (Egorov, 1991). However, long-term formation of carbonatite minerals also cannot be excluded.

The obtained age of 245 ± 3 Ma (Fig. 3a) contains unknown geologic noise, which is reflected in the value of MSWD = 22; such a result cannot be accepted as a reliable estimate of the age of the Od-16-19 carbonatite, let alone the Odikhincha massif as a whole. The arrangement of data points on the “residue plot” (Fig. 3b) does not contradict the fact that the age of carbonatite is close to 250 Ma, but most of the results of isotopic analysis of minerals are rejuvenated due to their prolonged crystallization from the melt/fluid.

Among other things, Fig. 3 clearly shows that two-point Rb–Sr isochrones made of mineral pairs or a mineral and whole rock, as well as isochrones with the slope determined by only one mineral with a high Rb/Sr ratio, in the case of disturbance of the closed isotopic system of phlogopite or other high rubidium mineral are prone to errors, far beyond those of measured isotopic ratios. Thus, Bagdasaryan et al. (2022) estimated the age of Odikhincha carbonatite as 258.0 ± 0.6 Ma from calcite, phlogopite, and heavy fraction (apatite). Note that recalculation with the

actual ^{87}Rb decay constant (Villa et al., 2015) gives an age of 262.3 ± 0.7 Ma, although this discrepancy is hardly significant considering the scatter of analytical points for the phlogopite fractions presented in Fig. 3. The individual age values calculated for each of our phlogopite analyses in Fig. 3 relative to calcite vary in a very wide range from 231 to 255 Ma. If the Rb–Sr system in the minerals of other carbonatite samples from the Maimecha-Kotui province is disturbed to the same extent as in sample Od-16-19, the published Rb–Sr age values (Bagdasaryan et al., 2022) are bound to contain an error. This error could also be inferred from the high MSWD value (58) for the isochron constructed for mineral and whole rock fractions of apatite aegirinite of the Magan Massif, indicating the age of 247 ± 7 Ma (Bagdasaryan et al., 2022).

U–Pb Dating and Corrections for Common Lead

The meaning of the U–Pb dates obtained for perovskite and titanite can be inferred from comparison with other geochronological data on rocks and minerals of the Odikhincha massif. A significant part of published geochronological data was obtained by U–Pb method for accessory minerals (perovskite, titanite, garnet, etc.) containing a certain proportion of common lead, which required appropriate corrections. Let us briefly consider potential sources of errors arising from such corrections.

Among the aforementioned accessory minerals, perovskite typically has the highest proportion of common lead (Kramers and Smith, 1983; Heaman, 1989; Wu et al., 2013; Anosova et al., 2019; Reguir et al., 2021), which often prevents accurate dating by local analysis performed via laser ablation or secondary ion mass spectrometry. The conventional ID-TIMS technique with correction for common lead using the ^{204}Pb signal (Kramers and Smith, 1983; Heaman, 1989; Kamo et al., 2003; Reguir et al., 2021) at first glance allows obtaining much smaller error values, but even in this case the dates are highly dependent on the method of correction for common lead, first of all, on the assumptions of its isotopic composition during the mineral formation, sometimes very controversial. In such cases, the seemingly high accuracy of the geochronological results can be deceptive. Model composition of lead is often used to make corrections. For instance, bounding the discordia in Fig. 4a to the isotopic ratio $^{207}\text{Pb}/^{206}\text{Pb} = 0.852$ corresponding, according to (Stacey and Kramers, 1975), to the composition of common lead as of 250 Ma ago, would shift the age of perovskite to 266 ± 4 Ma, which, in our opinion, indicates with a high degree of certainty that such an approach to correction for ordinary lead is not right.

The scale of $^{207}\text{Pb}/^{206}\text{Pb}$ isotopic ratio variations in the source of Siberian traps and alkaline rocks are shown in Fig. 6. They are several times wider than the Stacey–Kramers model variations for the entire Pha-

nerozoic; data points do not appear to cluster around 250 Ma on this model curve. In addition, the entire data set, including MORBs, is noticeably off the model line, i.e., this model does not reflect the source composition of these rocks. Therefore, correction for common lead with isotopic composition predicted by the Stacey–Kramers model (Salnikova et al., 2019; Reguir et al., 2021; Bagdasaryan et al., 2022) can obviously lead to significant age distortions; the probability of a random coincidence of the model lead isotopic composition with its real composition in the parent melt is negligible. The possible age distortion will be greater with a higher fraction of common lead in the sample. It should also be understood that correcting for common lead in classical ID–TIMS analysis and “binding” discordia to a fixed $^{207}\text{Pb}/^{206}\text{Pb}$ ratio on the ordinate axis in case of local analysis by the LA–ICP–MS or SIMS methods are essentially the same procedure, which, therefore, can in both cases lead to uncontrollable errors in seemingly accurate age determination.

To make corrections for common lead, its isotopic composition can be established when analyzing syngenetic equilibrium uranium-free minerals (Kamo et al., 2003), but it is also worthwhile to make sure that different mineral phases contain homogeneous lead, with the same initial isotopic ratios. Otherwise, the dating accuracy may again be overestimated.

The most reliable method for making corrections for common lead is the 3D discordia method (Ludwig, 2003), however, required precision of ^{204}Pb measurements is beyond the ability of most analytical instruments.

The U–Pb System in Carbonatite Minerals

The U–Pb system in carbonatite minerals studied in the present work is as far from the ideal as Rb–Sr: it is complicated by both disturbance of the isotopic system and, as noted above, the presence of a large amount of common lead in both titanite and perovskite (Fig. 4).

The high and weakly varying fraction of common lead in perovskite makes points on the diagram with concordia (Fig. 4a) lie rather compactly. The angular coefficient of the discordia drawn through them has, thus, relatively wide variations and the obtained age value in turn has a large error, 247 ± 18 Ma.

U–Pb data on titanite (Fig. 4b) also suggest the presence of common lead. Titanite usually contains less common lead than perovskite, and the fraction of radiogenic lead can sometimes approach 100% (Simonetti et al., 2006; Storey et al., 2006), as observed in Fig. 4b. Discordia drawn through the points corresponding to the titanite analyses allow the U–Pb system closure time in this mineral to be estimated at 244 ± 5 Ma.

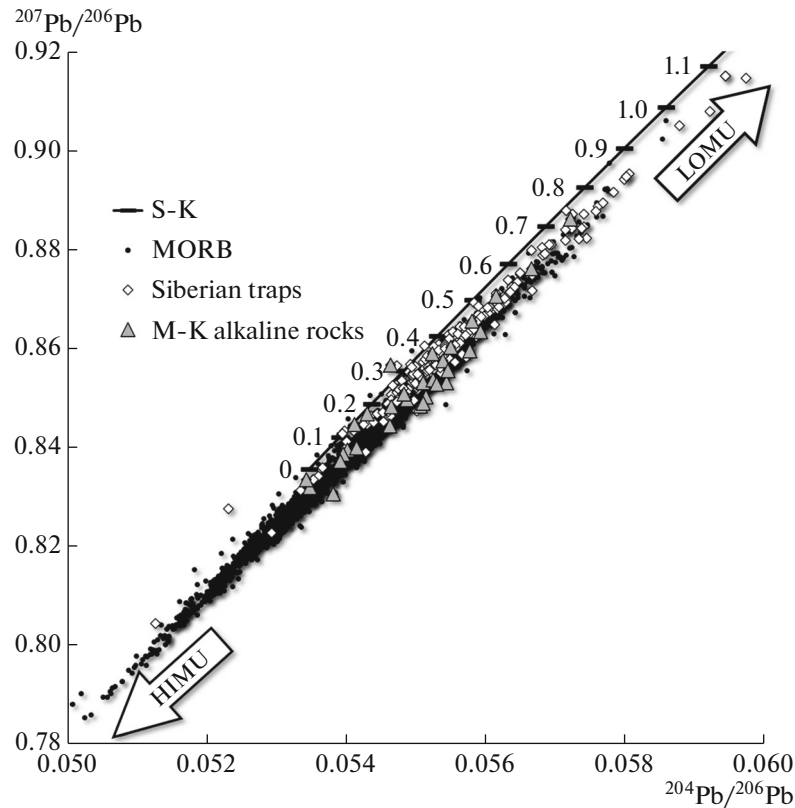


Fig. 6. Variations of lead isotopic composition in Siberian traps (Sharma et al., 1992; Lightfoot et al., 1993; Wooden et al., 1993; Czamanske, 2002; Arndt et al., 2003; Carlson et al., 2006; Krivolutsкая, Rudakova, 2009; Malich et al., 2010; Krivolutsкая et al., 2012) and alkaline rocks of the Maimecha-Kotui complex (M-K alkaline rocks) (Sharma et al., 1992; Carlson et al., 2006; Kogarko and Zartman, 2007). For comparison, we also plotted data for MORB (Kostitsyn, 2004, 2007) and model source (S-K) composition (Stacey and Kramers, 1975). The numbers near the curve correspond to the model age of lead in billion years according to the Stacey–Kramers model. Directions for source compositions with high (HIMU) and low (LOMU) U/Pb ratios are also shown.

The U–Pb dates obtained for perovskite and titanite are generally close to the value of 245 ± 3 Ma for Rb–Sr obtained for phlogopite and calcite from the same carbonatite sample. As was discussed above, the Rb–Sr system of the minerals was most likely disturbed in the course of their prolonged formation, including its metasomatic stage. The U–Pb systems of perovskite and titanite might have been similarly affected by prolonged crystallization of carbonatite minerals, and so we believe that both Rb–Sr and U–Pb isotope systems in the Od-16-19 carbonatite minerals reflect the time of the metasomatic process rather than the primary crystallization of carbonatite.

More accurate geochronological data were obtained for Odikhincha by Salnikova et al., (2019). Two garnet fractions from late pegmatoidal veins of alkaline composition were dated by the conventional U–Pb method, and, after minor corrections for common lead, a concordant age value of 249.8 ± 0.5 Ma was obtained. This result is probably in the best agreement with the data of Kamo et al. (2003) for the Arydzhang Formation (251.7 ± 0.4 Ma), which is believed to be the closest in time to the formation of intrusive rocks of the Maimecha-Kotui Complex.

Earlier geochronologic data for Odikhincha are rather controversial. K–Ar dates of 255 ± 10 and 256 ± 10 Ma, obtained, respectively, for nepheline from urtite and melteigite in one of the oldest works on Odikhincha massif geochronology (Kononova et al., 1973), overlap within error bars with both our results and those of (Salnikova et al., 2019). K–Ar ages of 262 ± 8 and 264 ± 8 Ma obtained, respectively, for phlogopite from carbonatite and from phlogopitized olivinite, on the other hand, do not fit into the expected sequence of events.

Bagdasaryan et al. (2022) published a U–Pb age of 266 ± 29 Ma obtained by laser ablation for apatite with abundant common lead and a ^{40}Ar – ^{39}Ar age of 267 ± 5 Ma for phlogopite from the same sample.

Parent Melt Sources

Problem of Enriched and Depleted Mantle Sources

The isotopic data presented in Table 5 and Fig. 5 show that the rocks of even such a relatively small magmatic body as the Odikhincha massif are isotopically heterogeneous: the values of $\epsilon_{\text{Nd}}(\text{T})$ vary from

+1.1 to +4.5, $(^{87}\text{Sr}/^{86}\text{Sr})_0$ from 0.7033 to 0.7046. Many authors associate Nd isotopic ratios with positive $\epsilon_{\text{Nd}}(\text{T})$ with depleted mantle sources. Thus, Kogarko and Zartman (2007, 2011), analyzed variations in the Nd–Sr–Pb isotopic composition of the rocks of the Gulinsky Massif and concluded that one of the sources of the parent melts was the depleted mantle. The now-conventional assumption that rocks having $\epsilon_{\text{Nd}}(\text{T})$ above zero are to be straightforwardly attributed to the chondritic homogeneous reservoir (CHUR), originates from (DePaolo and Wasserburg, 1976) An actually positive $\epsilon_{\text{Nd}}(\text{T})$ means that the source of the given rock had an elevated Sm/Nd ratio (low La/Lu), which corresponds to depleted matter characteristics. A negative $\epsilon_{\text{Nd}}(\text{T})$, on the other hand, means that the Sm/Nd ratio in the source was low (high La/Lu), which corresponds to geochemically enriched matter. The relevant question here is about the reference point, the primitive composition relative to which a particular substance is considered as depleted or enriched. DePaolo and Wasserburg suggested it to be chondrite (CHUR) with Sm/Nd = 0.325.

The evidence for the existence of CHUR in the Earth's interior is based, as we now realize, on completely unreliable material. DePaolo and Wasserburg (1976) had furnished the evolutionary line of chondrites with points corresponding to the modern basalt of the Columbia River Formation (BCR-1), diabase of the Rhodesian Great Dyke (RHO), and two samples of rocks of acidic composition, granodiorite RN3 from the Preisak-Lakorn batholith within the province of Superior, Canada, and gneiss (OGG) of granodiorite composition of the Amitsoq Formation of West Greenland.

Obviously, the granodiorites fell on the evolutionary line of the chondrites by chance, because these rocks were definitely not of mantle origin. Isotopic exploration of the Great Dyke of Rhodesia has shown that constituent gabbro-diabases have an $\epsilon_{\text{Nd}}(\text{T})$ value varying from -0.03 to $+4.68$ (Oberthür et al., 2002); i.e., the corresponding point fell on the CHUR line again by chance. Finally, extensive isotopic studies of Miocene Columbia River basalts, part of a giant magmatic province in western North America, have also shown their extremely high isotopic heterogeneity (Carlson et al., 1981; Brandon et al., 1993; Hooper and Hawkesworth, 1993; Day et al., 2021), with $\epsilon_{\text{Nd}}(\text{T})$ ranging from -17 to $+7.8$. Thus, the evidence that the Earth's primitive mantle corresponds to a chondritic homogeneous reservoir is based on four random analytical points, two of which had no mantle source, while the other two represented very heterogeneous mantle-originated formations. Thus, to the best of our knowledge, the assumption that the Earth's mantle and CHUR are identical in the Sm–Nd isotope characteristics is unfounded. It has also never been confirmed later. The discrepancy between the composition of the Earth's mantle in the Sm–Nd and Lu–Hf

isotope systems and the chondritic homogeneous reservoir is discussed in more detail in (Kostitsyn, 2004), where, in particular, it is shown that the present-day composition of the primitive mantle in the Sm–Nd isotope system is close to $\epsilon_{\text{Nd}}(0) \approx +9$ and Sm/Nd ≈ 0.350 . Accordingly, higher neodymium isotopic ratios correspond to depleted sources, and lower ones to enriched ones.

The superchondritic Sm/Nd ratio of the primitive mantle is also indicated by short-lived ^{146}Sm – ^{142}Nd isotope system (Boyet and Carlson, 2005; Caro et al., 2008; Frossard et al., 2022), with the short half-life of ^{146}Sm definitely indicating that the differences in the Sm/Nd ratio between the silicate part of the Earth and the chondrites arose at the stage of planetary-system formation rather than as a result of differentiation of the terrestrial matter.

As a result, the evolution line of primitive mantle sources that divides the compositions into depleted (above the line) and enriched (below the line) should have been characterized by the parameters $\epsilon_{\text{Nd}}(0) \approx +9$ and Sm/Nd ≈ 0.350 .

Sources of Odikhincha Parent Melts

The Sr and Nd isotopic ratios of the studied rocks of the alkaline–ultrabasic formation, as noted above, indicate a relatively enriched source of their parent melts (Fig. 5b) in comparison with the composition of the convective mantle, represented by its globally widespread products of magmatism in the form of basalts of mid-ocean ridges. That is, the source of the magmas that formed the Odikhincha massif and volcanics of the Arydzhang Formation had an enriched component, which for a long time had lower Sm/Nd ratios and higher Rb/Sr values, as indicated by slightly higher strontium isotopic ratios and markedly lower neodymium isotopic ratios in these rocks as compared to MORBs.

The nature of the enriched component in the source of Maimecha-Kotui ultramafic–alkaline rocks can be conventionally inferred from the following considerations. The arrows in Fig. 5b show the trends for neodymium and strontium isotopic ratios in three potential types of enriched rocks that could be present in the basement of the Siberian Platform. These could be rocks once separated from the convective mantle, (i) corresponding to the median continental crust (CC) composition as estimated by (Taylor and McLennan, 1985) or magmatic rocks of mantle origin, among which we consider two potential contrasting groups of (ii) tholeiitic and (iii) alkaline composition. The data used to obtain median estimates of these igneous rocks were taken from the isotope-geochemical database (Kostitsyn, 2004, 2007). The geochemical parameters of these enriched sources together with the composition of the convective mantle are summarized in Table 6.

Table 6. Model sources

Model source	Rb/Sr	Sm/Nd
Convective mantle (MORB) (Kostitsyn, 2004)	0.020	0.350
Continental crust (Taylor and McLennan, 1985)	0.123	0.219
Continental tholeiites:		
Median (second quartile)	0.059	0.258
First and third quartile	0.028–0.105	0.233–0.284
N =	11829	6702
Continental alkaline rocks:		
Median (second quartile)	0.045	0.180
First and third quartile	0.026–0.080	0.146–0.212
N =	743	477

The arrows and scatter sectors in Fig. 5b are plotted assuming that the rocks separated from the convective mantle initially had Nd and Sr isotopic ratios corresponding to this source, but, with time, their isotopic ratios become anomalous due to radioactive decay of ^{147}Sm and ^{87}Rb the more strongly, the more time has passed since the separation of the rock from the mantle source and the more the Rb/Sr and Sm/Nd ratios differ from the mantle ones.

To visualize the chemical heterogeneity of these enriched sources by Rb/Sr and Sm/Nd ratios, which, in time, determines their isotopic heterogeneity, we used the values of the first and third quartiles of the set of values available in our database (Table 6). It would be wrong to use such parameters as the mean and standard deviation for these purposes because the statistical distributions of trace elements contents in igneous rocks are not Gaussian (Kostitsyn, 2007) and the ratios of these elements do not obey the normal law. In this case, nonparametric statistics should be applied. We used the median values of the samples to characterize the central value of the Rb/Sr and Sm/Nd ratios (Table 6) and the first and third quartiles to characterize the scatter. It should be also borne in mind that only 50% of the data are between the first and third quartiles, while 25% of them are below the first and above the third quartile. Therefore, the variation ranges of elemental ratios in Table 6 and the boundaries of the scatter sectors in Fig. 5b are not exactly accurate.

Figure 5b shows that most of the data on the Siberian traps lie between the trends corresponding to the enriched sources of tholeiitic basalts and the average composition of the continental crust according to (Taylor and McLennan, 1985); i.e., these two types of compositions could be present in the source of their parent melts as enriched components. The points corresponding to alkaline intrusive rocks of the Odikhincha and volcanics of the Arydzhang Formation in Fig. 5b lie between the Thol and Alk trends; i.e., the enriched components in their source could be represented predominantly by ancient basic rocks of tholeiitic and

alkaline compositions. The influence of the component corresponding to the average composition of the continental crust in their source is clearly insignificant. It is also evident from this figure that the Devonian dolomites could not be the source of carbonate matter of the Odikhincha carbonatites, especially taking into account the much lower contents of neodymium and strontium in sedimentary dolomites in comparison with the Odikhincha carbonatites (Table 5).

Note that the Rb/Sr and Sm/Nd ratios in individual analyses of alkaline and tholeiitic basalts vary widely and overlap to a large extent, but the median and mean values differ markedly and regularly (Table 6). This gives us grounds to suppose that the alkaline igneous rocks of the Maimecha-Kotui Province could have formed from the melt that inherited composition of the enriched older alkaline component.

We can approximately estimate the time of formation of these enriched source rocks based on the values of the two-stage Sm/Nd model ages of the studied samples, which vary from 0.63 to 0.96 Ga (Table 5). However, it should be kept in mind that the age for the first stage of the two-stage model, i.e., the stage of evolution of the parent melt source, is calculated using the value of the Sm/Nd ratio of the continental crust. If the predominant enriched component in the source of the Odikhincha and Arydzhang parental melts corresponded to alkaline rocks, i.e., had a slightly lower value of Sm/Nd ratio (0.180) compared to the continental crust (0.219), the estimate of the time of separation of this component from the convective mantle should be somewhat lower, 0.55–0.80 Ga. The enriched tholeiitic component, however, which could also have been in the source of these rocks (Fig. 5b), has, in contrast, a higher Sm/Nd ratio (0.258), and, thus, the mixture of alkaline and nonalkaline enriched components may not have differed significantly in Sm/Nd ratio from the average crustal one and then the model age estimates for the enriched source in Table 5 do not appear to be significantly distorted.

Local Variations of Sr and Nd Isotopic Composition within the Massif

In general, the variations of Sr and Nd isotopic composition in the samples of the Odikhincha massif do not vary widely. However, even these variations show some kind of pattern.

First of all, it should be pointed out that nepheline-bearing rocks are more homogeneous in terms of the initial neodymium isotopic ratio than melilite-bearing rocks (Fig. 5a). No such distinction is shown by the strontium isotopic composition, which may be related to the generally wider variations in the initial isotopic composition of strontium (compared to the measurement errors of isotopic ratios of these elements). Nepheline-bearing rocks both at the Odikhincha massif and other massifs of the Maimecha-Kotui Province are later formations compared to melilite-bearing rocks (Egorov, 1969, 1991). It is possible that the neodymium isotopic composition was levelling in the process of evolution of parental magmas from early to late magmatic stages.

The Arydzhang volcanics also fall into two groups according to the neodymium isotopic composition. Limburgite, picrite, and olivine melilitite contain neodymium with higher $\epsilon_{Nd}(T)$ values, whereas melanephelinite, including melilite-bearing melilitite, coincides in $\epsilon_{Nd}(T)$ with nepheline-bearing Odikhincha rocks.

As was discussed above, variations of the initial isotopic ratio of neodymium in melilite-bearing and earlier rocks (olivinites, pyroxenites) vary within not very wide limits, $\epsilon_{Nd}(T)$ varies from +1.7 to +4.5. However, even these small variations show spatial regularity. Figure 7 shows the distribution of Nd (Fig. 7a) and Sr (Fig. 7b) isotopic ratios as a function of the distance of the sampling point to the middle of the depression (so-called "cirque") in the central part of the massif. The samples from the central part of the cirque (pyroxenite Od-7-14, carbonatite Od-8-14, uncompahgrite Od-9-14, and okaite Od-10-14) have the highest neodymium isotopic ratios of the whole collection, and, in the other rock samples, the neodymium isotopic ratios decrease smoothly with distance from the middle of the cirque (Fig. 7a), in any direction (Fig. 2). The same rocks from the central part of the cirque listed above have the lowest strontium isotopic ratios (Fig. 7b), although the relative variations of strontium isotopic ratios of the other samples are much wider than in Fig. 7a.

This distribution of Nd isotopic ratios agrees with the known symmetrical structure of most massifs of the Maimecha-Kotui province, which were formed as intrusive bodies of the central type, i.e., stocks complicated by annular or semi-annular bodies of later intrusion phases (Egorov, 1991). The example of Odikhincha shows that rocks at the center of the massif are characterized by the most primitive (mantle) isotopic ratios of neodymium and strontium, while the contribution of enriched component increases to the periphery. Appar-

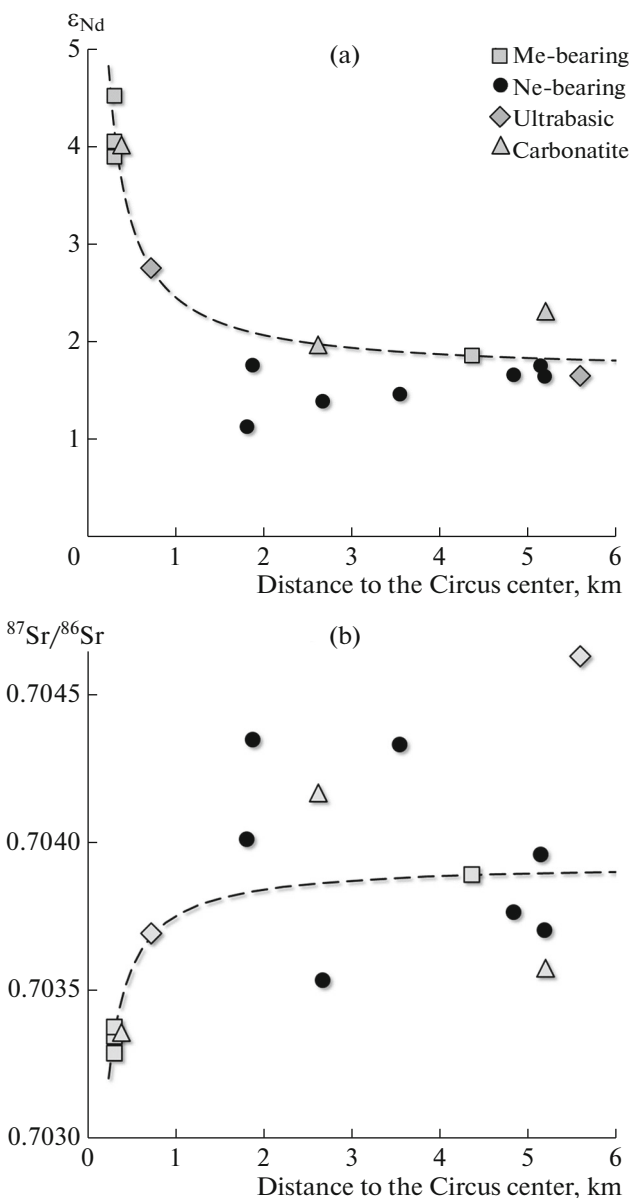


Fig. 7. Dependence of initial isotopic ratios of (a) neodymium and (b) strontium on the distance to the central part of the cirque on Mount Odikhincha. Melilite- (Me) bearing rocks along with part of carbonatites and ultrabasic rocks form a hyperbolic curve, while nepheline- (Ne) bearing rocks do not follow this geographic dependence.

ently, the parent melt of mantle origin, as it moved to the top of the continental lithosphere, assimilated its matter that had more enriched isotopic characteristics compared to its initial isotopic composition.

CONCLUSIONS

The Rb–Sr isotope system of phlogopite and calcite from carbonatite Od-16-19 of Odikhincha massif is disturbed; the age of 245 ± 3 Ma, obtained from mineral isochrone appears to be close to the time of

formation of Siberian traps and rocks of ultrabasic–alkaline Maimecha–Kotui complex; however, a large scatter of analytical points (MSWD = 22) cast doubts on its reliability. The disturbance of the isotopic system is probably due to the strontium isotopic composition changing during autometasomatic phlogopitization of carbonatite.

The U–Pb isotopic system of titanite and perovskite from the same carbonatite sample also turned out to be disturbed, since analytical points form discordia. The U–Pb dates obtained for titanite and perovskite were 244 ± 5 (MSWD = 1.8) and 247 ± 18 Ma (MSWD = 4), respectively.

Apparently, consistent dates obtained for both isotopic systems (245 ± 3 Ma by Rb–Sr and 247 ± 18 , 244 ± 5 Ma by U–Pb) reflect the time of metasomatism (phlogopitization and iolitization), widely manifested in the rocks of the Odikhincha massif.

The presented Rb–Sr and Sm–Nd isotope data for ultrabasic–alkaline intrusive rocks with carbonatites of the Odikhincha massif and volcanics of the Arydzhang Formation indicate an enriched, relative to the composition of the convective mantle, and isotopically heterogeneous source of their parent melts. This source could be a combination of ultrabasic mantle rocks and rocks of basic composition (basites). The latter played the role of an enriched component.

There were no signs of in situ melt contamination by the host sedimentary rocks, however, variations of strontium and neodymium isotopic ratios in the rocks of the Odikhincha massif may indicate interaction and material exchange of ascending deep magmas with the surrounding rocks of the lithosphere and the Earth's crust in the course of the massif emplacement up to its complete solidification.

ACKNOWLEDGMENTS

The authors are grateful to Yu.D. Gritsenko and O.I. Gritsenko for their help with fieldwork in the summer of 2019, as well as to two anonymous reviewers and A.V. Chugaev, whose comments helped improve the manuscript. We are also thankful to K.M. Ryazantsev for his help with electron microscope analyses.

FUNDING

This work was performed in the framework of state orders to the Vernadsky Institute of Geochemistry and Analytical Chemistry, Russian Academy of Sciences, and Institute of Geology of Ore Deposits, Petrography, Geochemistry and Mineralogy, Russian Academy of Sciences.

CONFLICT OF INTEREST

The authors of this work declare that they have no conflicts of interest.

OPEN ACCESS

This article is licensed under a Creative Commons Attribution 4.0 International License, which permits use, sharing, adaptation, distribution and reproduction in any medium or format, as long as you give appropriate credit to the original author(s) and the source, provide a link to the Creative Commons license, and indicate if changes were made. The images or other third party material in this article are included in the article's Creative Commons license, unless indicated otherwise in a credit line to the material. If material is not included in the article's Creative Commons license and your intended use is not permitted by statutory regulation or exceeds the permitted use, you will need to obtain permission directly from the copyright holder. To view a copy of this license, visit <http://creativecommons.org/licenses/by/4.0/>.

REFERENCES

- C. Alibert, A. Michard, and F. Albarede, “The transition from alkali basalts to kimberlites: isotope and trace element evidence from melilitites,” *Contrib. Mineral. Petrol.* **82**, 172–186 (1983).
- M. Anosova, Y. A. Kostitsyn, and L. Kogarko, “Correlation of high-calcium silica-undersaturated complex of the Maymecha–Kotuy Province with Siberian flood basalts: new age data on the Kugda Massif (Polar Siberia),” *Geochem Int.* **57** (12), 1339–1342 (2019).
- N. Arndt, C. Chauvel, G. Czamanske, and V. Fedorenko, “Two mantle sources, two plumbing systems – tholeiitic and alkaline magmatism of the Maymecha River basin, Siberian Flood Volcanic Province,” *Contrib. Mineral. Petrol.* **133** (3), 297–313 (1998).
- N. T. Arndt, G. K. Czamanske, R. J. Walker, C. Chauvel, and V. A. Fedorenko, “Geochemistry and origin of the intrusive hosts of the Noril'sk–Talnakh Cu–Ni–PGE sulfide deposits,” *Econ. Geol.* **98** (3), 495–515 (2003).
- T. E. Bagdasaryan, S. N. Thomson, A. V. Latyshev, R. V. Veselovskiy, V. A. Zaitsev, A. E. Marfin, V. S. Zakharov, and D. S. Yudin, “Thermal history of the Siberian Traps Large Igneous Province revealed by new thermochronology data from intrusions,” *Tectonophysics* **836**, 229385 (2022).
- M. Boyet and R. W. Carlson, “ ^{142}Nd evidence for early (>4.53 Ga) global differentiation of the Silicate Earth,” *Sci.* **309**, 576–571 (2005).
- A. D. Brandon, P. R. Hooper, G. G. Goles, and R. S. Lambert, “Evaluating crustal contamination in continental basalts – the isotopic composition of the Picture Gorge Basalt of the Columbia River Basalt Group,” *Contrib. Mineral. Petrol.* **114** (4), 452–464 (1993).
- E. L. Butakova and L. S. Egorov, “Maymecha–Kotui complex of the formation of alkaline and ultrabasic rocks,” *Petrography of East Siberia (AN SSSR, 1962)*, pp. 417–589 [in Russian].
- R. W. Carlson, G. W. Lugmair, and J. D. Macdougall, “Columbia River volcanism: the question of mantle heterogeneity or crustal contamination,” *Geochim. Cosmochim. Acta.* **45** (12), 2483–2499 (1981).
- R. W. Carlson, G. Czamanske, V. Fedorenko, and I. Ilupin, “A comparison of Siberian meimechites and kimberlites: Implications for the source of high–Mg alkalic

- magmas and flood basalts,” *Geochem., Geophys., Geosyst.* **7** (11), (2006)
- G. Caro, B. Bourdon, A. N. Halliday, and G. Quitte, “Super-chondritic Sm/Nd ratios in Mars, the Earth and the Moon,” *Nature* **452** (7185), 336–339 (2008).
- G. K. Czamanske, “Petrographic and geochemical characterization of ore-bearing intrusions of the Norilsk type, Siberia; with discussion of their origin, including additional datasets and core logs,” *US Geol. Surv. Publ. Open-File Report 74*, (2002).
- J. A. Dalton and D. C. Presnell, “Carbonatitic melts along the solidus of model ilherzolite in the system CaO–MgO–Al₂O₃–SiO₂–CO₂ from 3 to 7 GPa,” *Contrib. Mineral. Petrol.* **131**, 123–135 (1998).
- J. A. Dalton and B. J. Wood, “The compositions of primary carbonate melts and their evolution through wallrock reaction in the mantle,” *Earth Planet. Sci. Lett.* **119** (4), 511–525 (1993).
- J. M. Day, K. L. Nutt, B. Mendenhall, and B. J. Peters, “Temporally variable crustal contributions to primitive mantle-derived Columbia River Basalt Group magmas,” *Chem. Geol.* **572**, 120197 (2021).
- D. J. DePaolo and G. J. Wasserburg, “Nd isotopic variations and petrogenetic models,” *Geophys. Res. Lett.* **3** (5), 249–252 (1976).
- L. S. Egorov, *Melilitic Rocks of the Maymecha–Kotuy Province* (Nedra, Leningrad, 1969) [in Russian].
- L. S. Egorov, *Iolite–Carbonatite Plutonism: Evidence from the Maymecha–Kotui Complex of the Polar Uras* (Nedra, Leningrad, 1991).
- R. E. Ernst and K. Bell, “Large igneous provinces (LIPs) and carbonatites,” *Mineral. Petrol.* **98** (1), 55–76 (2010).
- V. Fedorenko, G. Czamanske, T. Zen’ko, J. Budahn, and D. Siems, “Field and geochemical studies of the melilite-bearing Arydzhangsky Suite, and an overall perspective on the Siberian alkaline-ultramafic flood-volcanic rocks,” *Int. Geol. Rev.* **42** (9), 769–804 (2000).
- P. Frossard, C. Israel, A. Bouvier, and M. Boyet, “Earth’s composition was modified by collisional erosion,” *Science* **377** (6614), 1529–1532 (2022).
- C. J. Hawkesworth, P. C. Lightfoot, V. A. Fedorenko, S. Blake, A. J. Naldrett, W. Doherty, and N. S. Gorbachev, “Magma differentiation and mineralization in the Siberian continental flood basalts,” *Lithos* **34** (1–3), 61–88 (1995).
- L. M. Heaman, “The nature of the subcontinental mantle from SrNdPb isotopic studies on kimberlitic perovskite,” *Earth Planet. Sci. Lett.* **92** (3–4), 323–334 (1989).
- P. R. Hooper and C. J. Hawkesworth, “Isotopic and geochemical constraints on the origin and evolution of the Columbia River Basalt,” *J. Petrol.* **34** (6), 1203–1246 (1993).
- A. Ivanov, F. Corfu, V. S. Kamenetsky, A. Marfin, and N. Vlydykin, “²⁰⁷Pb-excess in carbonatitic baddeleyite as the result of Pa scavenging from the melt,” *Geochem. Perspect. Lett.* **18**, 11–15 (2021).
- S. L. Kamo, G. K. Czamanske, Y. Amelin, V. A. Fedorenko, D. Davis, and V. Trofimov, “Rapid eruption of Siberian flood-volcanic rocks and evidence for coincidence with the Permian–Triassic boundary and mass extinction at 251 Ma,” *Earth Planet. Sci. Lett.* **214** (1–2), 75–91 (2003).
- A. I. Kiselev, V. V. Yarmolyuk, M. D. Tomshin, A. V. Niki-forov, and K. N. Egorov, “Permian-triassic traps of the East Siberian Craton: The problem of estimation of the sources of Phanerozoic intraplate magmatism,” *Dokl. Earth Sci.* **455** (1), 299–305 (2014).
- L. N. Kogarko and R. E. Zartman, “A Pb isotope investigation of the Guli massif, Maymecha–Kotuy alkaline-ultramafic complex, Siberian flood basalt province, Polar Siberia,” *Mineral. Petrol.* **89** (1), 113–132 (2007).
- L. Kogarko and R. Zartman, “New data on the age of the Guli intrusion and implications for the relationships between alkaline magmatism in the Maymecha–Kotuy province and the Siberian superplume: U–Th–Pb isotopic systematics,” *Geochem. Int.* **49** (5), 439 (2011).
- L. Kogarko, S. Karpenko, A. Lyalikov, and M. Teptev, “Isotope criteria for genesis of meymechite magmatism,” *Dokl. Akad. Nauk SSSR* **301**, 939–942 (1988).
- L. N. Kogarko, V. A. Kononova, M. P. Orlova, and A. R. Wooley, *Alkaline Rocks and Carbonatites of the World. Part 2. Former USSR* (Chapman and Hall, London, 1995).
- V. A. Kononova, L. L. Shanin, and M. M. Arakelyants, “Timing of alkaline massifs and carbonatites,” *Izv. Akad. Nauk SSSR, Ser. Geol.*, No. 5, 25–36 (1973).
- Yu. A. Kostitsyn, “Terrestrial and chondritic Lu–Hf and Sm–Nd isotopic systems: are they identical?,” *Petrology* **12** (5), 397–411 (2004).
- A. Yu. Kostitsyn, “Relationships between the chemical and isotopic (Sr, Nd, Hf, and Pb) heterogeneity of the mantle,” *Geochem. Int.* **45** (12), 1173–1196 (2007).
- Yu. A. Kostitsyn and M. O. Anosova, “U–Pb age of extrusive rocks in the Uxichan Caldera, Sredinnyi Range, Kamchatka: application of laser ablation in dating young zircons,” *Geochem. Int.* **51** (2), 155–163 (2013).
- J. D. Kramers and C. B. Smith, “A feasibility study of U–Pb and Pb–Pb dating of kimberlites using groundmass mineral fractions and whole-rock samples,” *Chem. Geol.* **41**, 23–38 (1983).
- N. A. Krivolutskaya and A. V. Rudakova, “Structure and geochemical characteristics of trap rocks from the Noril’sk Trough, Northwestern Siberian craton,” *Geochem. Int.* **47** (7), 635–656 (2009).
- N. Krivolutskaya, A. Sobolev, V. Mikhailov, A. Plechova, Y. A. Kostitsyn, I. Roschina, and Z. Fekiacova, “Parental melt of the Nadezhdinsky Formation: Geochemistry, petrology and connection with Cu–Ni deposits (Noril’sk area, Russia),” *Chem. Geol.* **302**, 87–105 (2012).
- P. C. Lightfoot, C. J. Hawkesworth, J. Hergt, A. J. Naldrett, N. S. Gorbachev, V. A. Fedorenko, and W. Doherty, “Remobilisation of the continental lithosphere by a mantle plume: major-, trace-element, and Sr-, Nd-, and Pb-isotope evidence from picritic and tholeiitic lavas of the Noril’sk District, Siberian Trap, Russia,” *Contrib. Mineral. Petrol.* **114** (2), 171–188 (1993).
- K. R. Ludwig, “Isoplot 3.00 – a geochronological toolkit for Microsoft Excel,” *Berkeley Geochronol. Center Spec. Publ.*, No. 4 (2003).
- K. Malitch, I. Badanina, and E. Tuganova, “Magmatic evolution of ultramafic-mafic intrusions of the Norisk province (Russia): composition and geochronological data,” *Litosfera*, No. 5, 37–63 (2010).

- T. Morikiyo, T. Miyazaki, H. Kagami, N. V. Vladykin, E. A. Chernyshova, L. I. Panina, N.M.P., “Sr, Nd, C and O isotope characteristics of Siberian carbonatites. Alkaline magmatism and the problems of mantle sources,” *International Workshop, Irkutsk, 2001* (Irkutsk, 2001), pp. 69–84.
- T. Oberthür, D. W. Davis, T. G. Blenkinsop, and A. Höhn-dorf, “Precise U–Pb mineral ages, Rb–Sr and Sm–Nd systematics for the Great Dyke, Zimbabwe—constraints on late Archean events in the Zimbabwe craton and Limpopo belt,” *Precambrian Res.* **113** (3–4), 293–305 (2002).
- B. Pokrovskiy and V. Vinogradov, “Isotope investigations on alkalic rocks of central and western Siberia,” *Int. Geol. Rev.* **33** (2), 122–134 (1991).
- S. N. Prokhorova, N. Z. Evzikova, and A. F. Mikhailova, *Phlogopite Content of the Maymecha–Kotuy Province of Ultrabasic Alkaline Rocks* (Nedra, 1966) [in Russian].
- E. P. Reguir, E. B. Salnikova, P. Yang, A. R. Chakhmouradian, M. V. Stifeeva, I. T. Rass, and A. B. Kotov, “U–Pb geochronology of calcite carbonatites and jacupirangite from the Guli alkaline complex, Polar Siberia, Russia,” *Mineral. Mag.* **85** (4), 469–483 (2021).
- M. K. Reichow, A. D. Saunders, R. A. Scott, I. L. Millar, D. Barfod, M. S. Pringle, N. W. Rogers, and S. Hammond, “Petrogenesis and timing of mafic magmatism, South Taimyr, Arctic Siberia: A northerly continuation of the Siberian Traps?,” *Lithos* **248–251**, 382–401 (2016).
- E. B. Salnikova, A. R. Chakhmouradian, M. V. Stifeeva, E. P. Reguir, A. B. Kotov, Y. D. Gritsenko, and A. V. Nikiforov, “Calcic garnets as a geochronological and petrogenetic tool applicable to a wide variety of rocks,” *Lithos*. **338**, 141–154 (2019).
- M. Sharma, A. R. Basu, and G. V. Nesterenko, “Temporal Sr-, Nd- and Pb-isotopic variations in the Siberian flood basalts: Implications for the plume-source characteristics,” *Earth Planet. Sci. Lett.* **113** (3), 365–381 (1992).
- A. Simonetti, L. M. Heaman, T. Chacko, and N. R. Banerjee, “In situ petrographic thin section U–Pb dating of zircon, monazite, and titanite using laser ablation–MC–ICP–MS,” *Int. J. Mass Spectrometry* **253** (1), 87–97 (2006).
- J. S. Stacey and J. D. Kramers, “Approximation of terrestrial lead isotope evolution by a two-stage model,” *Earth Planet. Sci. Lett.* **26**, 207–221 (1975).
- C. D. Storey, T. E. Jeffries, and M. Smith, “Common lead-corrected laser ablation ICP-MS U–Pb systematics and geochronology of titanite,” *Chem. Geol.* **227** (1–2), 37–52 (2006).
- S. R. Taylor and S. M. McLennan, *The Continental Crust: its Composition and Evolution* (Blackwell Sci., Oxford, 1985).
- van E. Achterbergh, C. G. Ryanm, and W. L. Griffin, “GLITTER: on-line interactive data reduction for the laser ablation ICP–MS microprobe,” *Proceedings of the 9th V.M. Goldschmidt Conference* (Cambridge, 1999).
- I. M. Villa, Bièvre P. De, N. Holden, and P. Renne, “IUPAC–IUGS recommendation on the half life of ^{87}Rb ,” *Geochim. Cosmochim. Acta* **164**, 382–385 (2015).
- J. L. Wooden, G. K. Czamanske, V. A. Fedorenko, N. T. Arndt, C. Chauvel, R. M. Bouse, B. S.W. King, R. J. Knight, and D. F. Siems, “Isotopic and trace-element constraints on mantle and crustal contributions to Siberian continental flood basalts, Norilsk area, Siberia,” *Geochim. Cosmochim. Acta* **57** (15), 3677–3704 (1993).
- F.-Y. Wu, A. A. Arzamastsev, R. H. Mitchell, Q.-L. Li, J. Sun, Y. -H. Yang, and R.-C. Wang, “Emplacement age and Sr–Nd isotopic compositions of the Afrikanda alkaline ultramafic complex, Kola Peninsula, Russia,” *Chem. Geol.* **353**, 210–229 (2013).
- D. York, “Least-squares fitting of a straight line. *Canad. J. Phys.* (21), 1079–1086 (1966).

Translated by M. Hannibal

Publisher’s Note. Pleiades Publishing remains neutral with regard to jurisdictional claims in published maps and institutional affiliations.